THE UNIVERSITY OF CALGARY

A PC-BASED UNIFIED GEOID FOR CANADA

by

BIN BIN SHE

A THESIS

SUBMITTED TO THE FACULTY OF GRADUATE STUDIES

IN PARTIAL FULFILLMENT OF THE REQUIREMENTS FOR THE

DEGREE OF MASTER OF SCIENCE IN ENGINEERING

DEPARTMENT OF GEOMATICS ENGINEERING

CALGARY, ALBERTA

APRIL, 1993

ISBN 0-315-83250-9

The UNIVERSITY OF CALGARY

FACULTY OF GRADUATE STUDIES

The undersigned certify that they have read, and recommend to the Faculty of Graduate Studies for acceptance, a thesis entitled "A PC-BASED UNIFIED GEOID FOR CANADA" submitted by Bin Bin She in partial fulfillment of the requirements for the degree of Master of Science in Engineering.

M G Sideris

Supervisor, Dr. M.G. Sideris, Department of Geomatics Engineering

K.P. Schwarz.

Dr. K.P. Schwarz, Department of Geomatics Engineering

Dr. G. Lachapelle, Department of Geomatics Engineering

Dr. S.T. Nichols, Department of Electrical and Computer Engineering

May 6, 1993

(Date)

ABSTRACT

Geoid determination is an important research area in geodesy. In this thesis, a PC-based software package, which incorporates the most recent developments in FFT-based techniques for geoid determination, has been developed. The software package can be used for computing large-scale continental geoids efficiently on low cost microcomputers. With the developed software package, a new high-precision geoid model (UC93) has been computed for all of Canada and part of the U.S., ranging from 35°N to 90°N in latitude and 210°E to 320°E in longitude. As compared to other existing geoids in North America, the new geoid model achieves the best agreement with the GPS/levelling data available in the region. Its absolute agreement with respect to the GPS/levelling datum is better than 10 cm RMS and the relative agreement is better than 15 cm, in most cases.

ACKNOWLEDGEMENTS

I wish to express my deep gratitude to my supervisor, Dr. Michael G. Sideris, for his continuous support and encouragement throughout the course of my graduate studies. His advice and help were essential for the completion of the thesis.

Special thanks go to Dr. K.P. Schwarz for his support and help during my graduate studies, and for his advice and critique on the research project related to this thesis. Dr. Gerald Lachapelle is gratefully thanked for providing financial assistance and supervision for the first year of my graduate studies. Mr. Yecai Li, Mr. Zuofa Li and Mr. Changyou Zhang are thanked for their willingness to discuss techniques and problems in geoid determination related to this research. I would also like to extend my appreciation to the Faculty, staff and fellow graduate students of the Department of Geomatics Engineering for making my studies enjoyable and productive.

Dr. A. Mainville and Mr. M. Veronneau of the Geodetic Survey Division of Canada, as well as Dr. D. Milbert of the U.S. National Geodetic Survey, are gratefully acknowledged for providing the data used in this research. Financial support came from a research project with the Geodetic Survey Division, E.M.R., Canada, an NSERC operating grant, and the University of Calgary in the form of Graduate Teaching and Research Assistantships. Their contributions are gratefully acknowledged.

Finally, I am very grateful to my wife Wuqing Yang for her patience and support during the course of my graduate studies.

TABLE OF CONTENTS

LIST OF TABLES

LIST OF FIGURES

Figure | Page

NOTATION

i) Symbols

c	terrain correction
c_n	anomaly degree variance
C_{nm}, S_{nm}	fully normalized spherical harmonic coefficients
E	planar area of integration
G	mean gravity
h	ellipsoidal height
H	orthometric height
j	the imaginary unit
k	wave number corresponding to x;
	Newton' gravitational constant
l	wave number corresponding to y; planar distance
m	wave number corresponding to u
M	record length along the x direction
n	wave number corresponding to v
N	record length along the y directon; geoidal undulation
N_{ind}	indirect effect of terrain reduction
N_d	direct effect of terrain reduction
N_{GM}	reference undulation
$N_{\Delta g}$	reference gravity anomaly
P	computation point
P_{nm}	fully normalized associated Legendre functions
Q	data point
R	Radius of the earth
T_x, T_y	periods along the x and y direction
u	spacial frequency corresponding to x
v	spacial frequency corresponding to y
x, y	Cartesian coordinates in x,y direction

Δg	gravity anomaly
ΔgGM	reference gravity anomaly
Δx	grid spacing in x direction
Δy	grid spacing in y direction
$\Delta\varphi$	grid spacing in latitude
$\Delta\lambda$	grid spacing in longitude direction
ε_n	anomaly error degree variance
γ	normal gravity
φ	latitude
λ	longitude
σ	standard deviation; spherical area of integration
σ^2	variance
ρ	density of topographical mass
ψ	spherical distance

ii) Defined Operators

$\mathbf{F}\,[\bullet]$	direct Fourier transform
$\mathbf{F}^{-1}\,[\bullet]$	inverse Fourier transform
$S\,(\bullet)$	Stokes' kernel function
$\leftrightarrow$	Fourier transform pair
$*$	convolution sign

iii)	**Acronyms**
CFT	continuous Fourier transform
DFT	discrete Fourier transform
E	East longitude
GM	global geopotential model

N	North latitude
eq.	equation
eqs.	equations
FFT	Fast Fourier Transform
GPS	Global Positioning System
RMS	root mean square
1D	one dimensional
2D	two dimensional

CHAPTER 1

INTRODUCTION

1.1 Background

With the advances of GPS techniques, it is now possible to obtain the ellipsoidal height (or geodetic height) with an accuracy of a few centimeters. The combination of the GPS-derived ellipsoidal heights with a gravimetric geoid of compatible accuracy could lead to the replacement of levelling as the main method to obtain the orthometric heights which are required for many engineering and scientific applications. The GPS/geoid approach would be more cost effective than conventional levelling while maintaining, in most cases, the same accuracy. In oceanography, a high-accuracy geoid combined with satellite altimetry data is required to obtain the sea surface topography which is important for studying ocean currents and other oceanographic phenomena. Therefore, the computation of a high-accuracy geoid is becoming increasingly important.

The basic method for geoid determination is the Stokes integral which is the solution of the third boundary value problem in physical geodesy (Heiskanen and Moritz, 1967). For local or regional geoid determination, the available discrete gravity anomaly data and height data are usually combined with a high degree geopotential model to generate the geoidal undulations through the remove-restore technique (Schwarz et al., 1990; Sideris and Forsberg, 1990). With this technique, the surface gravity anomaly data are first reduced to the geoid through a terrain reduction using the available height data and further reduced for the reference field contribution computed by the geopotential model. Then, the reduced anomaly data are used to generate the residual part of the geoid through the discrete Stokes integral. The final geoidal undulation will be the summation of the residual part, the reference undulation computed by the geopotential model, and the indirect effect obtained using height data.

Basically, there are two approaches to evaluate the discrete Stokes integral. The conventional approach is to evaluate the discrete Stokes integral directly through numerical integration or summation. The advantage of this approach is that it does not require gridded data and both mean and point data can be used conveniently. Since the numerical integration has to be done point by point with this approach, the computation is very time consuming especially when a large regional or continental geoid is to be computed. Usually one has to spend a lot of CPU time on large computers. In addition, the Stokes integral is usually truncated to a certain cap size and the information from data points outside the selected cap in the region is not used in this approach.

The second approach for evaluating the discrete Stokes integral is to use the fast Fourier transform (FFT) method. In addition to its speed, this technique allows for evaluation of the discrete Stokes integral for all the points on a regular grid using all the data available in a large region simultaneously. Therefore, it is an ideal approach for the determination of large-scale regional geoids, such as the Canadian geoid, in a unified way.

The first version of the FFT-based technique for evaluating the discrete Stokes integral is the planar FFT formula (Sideris and Schwarz, 1985; Schwarz et al., 1990). In this technique, the original Stokes integral, which is not a 2D convolution integral itself, is transformed to a 2D convolution by approximating the spherical Stokes kernel function with its planar approximation. This technique has been applied to compute quite a number of local or regional geoids both in and outside Canada (Sideris and Schwarz, 1985; Sideris et al., 1988a and 1988b; Denker, 1990; Forsberg, 1990; Veronneau and Mainville, 1991, etc.).

Due to the planar approximation, the geoid obtained by the above FFT technique is subject to an error which will increase with the integration area. To overcome this limitation, Strang van Hees (1990) put forward an approach which transforms the discrete Stokes integral to a 2D convolution by modifying Stokes' kernel function through spherical trigonometry and evaluates it directly on the sphere by 2D FFT. This technique has been successfully used to compute the U.S. continental geoid GEOID90 (Milbert, 1990). Due to the modification of Stokes' kernel function, this technique is subject to a latitude-dependent error which is not negligible for determining large-scale continental geoids. To reduce the effect of this latitude-dependent error, Forsberg and Sideris (1993) proposed an improved 2D (multi-band) spherical FFT approach. In this approach the whole grid is divided into a number of latitude bands of certain width with some overlap between neighbouring zones. The geoidal undulations are evaluated band by band by Strang van Hees' approach, thus reducing the latitude-dependent error significantly if the grid is divided into a sufficient number of bands.

The previous FFT-based techniques are approximations to the true discrete Stokes integral. To get rid of the approximations, Haagmanns et al. (1992) developed an approach called the 1D spherical FFT technique, which allows for evaluation of the true discrete Stokes integral parallel by parallel without any approximation. Another important advantage of this technique is that it just needs one dimensional complex arrays to perform the FFT operations, resulting in a considerable saving in computer memory. This makes it possible to compute large-scale continental geoids, such as the current Canadian geoid, efficiently even on microcomputers.

Another important development, which is essential to ensure the equivalence of the FFT-derived 2D or 1D discrete convolutions to those obtained through direct summation, is the proper use of zero padding of both the data grid and/or the kernel grid. Sideris and Li (1992 and 1993), Haagmans et al. (1993) have shown the effects of circular convolution on geoid determination and how they are eliminated by zero padding.

Up to now, the FFT-based techniques for evaluating convolutions in physical geodesy have been developed to such an extent that it is possible to evaluate the original discrete Stokes integral and other integrals, which are either 2D convolution integrals themselves or a linear combination of 2D convolutions, very efficiently by FFT without approximation. The algorithms can process large amounts of gridded data over large regions simultaneously. On the other hand, the developments in modern measurement techniques make it possible to extend and update the old data sets at a faster pace. Therefore, the development of efficient software which incorporates the theoretical and practical developments in the spectral techniques for evaluating the convolution integrals in physical geodesy on more cost-effective microcomputers is becoming increasingly important. Such a software package is especially important for geoid determination in Canada, which is the second largest country in the world with a 9.9 million km^2 territory.

In Canada, several gravimetric geoids have been computed using different techniques in the past few years. Vanicek et al. (1986, 1990) computed geoid models (UNB86 and UNB90) for the area 41°N - 72°N, 218°E - 314°E at a spacing of 10 arcminutes by direct numerical integration using Molodenskij's truncation method. Sideris and Schwarz (1985, 1988a and 1988b) computed local geoidal models for the provinces of Alberta and British Columbia using the planar FFT technique. In 1991, Veronneau and Mainville computed the GSD91 geoid model for Canada by means of the planar FFT technique using the newly gridded 5'x5' gravity anomaly data and 1kmx1km height data as well as the OSU91A geopotential model complete to degree and order 360. No zero padding was applied in the GSD91 geoid determination due to the limitation of computer memory (Veronneau and Mainville, 1992).

All these geoid models were computed on large computers and were subject to the various approximations mentioned before.

With the rapid expansion of applications of GPS positioning in Canada and the improvement of positioning accuracy, there is a demanding need for a unified gravimetric geoid of high accuracy to be used together with the GPS-derived heights to provide orthometric heights for various engineering and scientific users over vast areas in this country in a more cost effective way than conventional levelling.

1.2 Objectives of the Research and Outline of the Thesis

One of the major objectives of this research is to develop a PC-based software package for geoid determination which incorporates the most recent theoretical and practical developments in FFT-based techniques for evaluating various discrete convolution integrals related to geoid determination. The software package will include efficient PC-based programs for the rigorous evaluation of the discrete Stokes integral, the terrain corrections, and the ~~direct and~~ indirect effect of the terrain on the geoid efficiently by means of the 1D FFT technique using gridded data in very large continental areas such as all of Canada or even the whole of North America. It will also contain a program for error propagation, interpolation and graphical display of geoidal undulations.

Another major objective of this research is to produce a unified geoid of high accuracy for all of Canada and part of the U.S. (35°N - 90°N, 210°E -

320°E) at a spacing of 5 arcminutes (a total of 871200 grid points) and quantify its accuracy. The geoid will be available on floppy or optical disks together with the interpolation program and will be provided to various interested users in industry, government and scientific institutions in the region.

Chapter 2 describes the basic formulas and procedures for geoid determination. The fundamental formulas for geoid computation are first introduced. Then, the 1D and 2D continuous and discrete Fourier transform theory is briefly reviewed. Some of the important properties of the discrete Fourier transform are discussed with emphasis on the convolution theorem, addition theorem, as well as the relation between the 1D and 2D discrete convolutions. Practical formulas for evaluating various discrete integrals related to geoid determination by FFT in the frequency domain are introduced. Chapter 3 discusses the precision of the geoidal undulations by error propagation using the given a priori statistical error information of the data. Formulas for evaluating the contribution of the gravity anomaly noise to the standard deviation of the computed geoidal undulations by FFT are derived. Chapter 4 contains a brief description of the computer software developed in this research. Chapter 5 gives a description of the data sets used for computing the current Canadian geoid and various geoid files produced in this research. In Chapter 6, extensive comparisons are made between the newly computed gravimetric geoid and the GPS/levelling data to evaluate its absolute and relative accuracy. Other existing geoid models in the region are also included in the comparison. Some conclusions and recommendations are given in Chapter 7.

CHAPTER 2

FORMULAS FOR GEOID DETERMINATION

In this chapter, the formulas used for local or regional geoid computation in both the space domain and frequency domain are summarized. First, the remove-restore technique, which is widely used for local or regional geoid determination by combining a global geopotential model, topographical heights and gravity anomaly data, is reviewed. Then the 1D and 2D discrete Fourier transform and the properties closely related to their application in evaluating the convolution integrals involved with geoid determination are discussed. Finally, the various techniques for evaluating the discretized Stokes integral and other related discrete convolutions using gridded data by fast Fourier transform (FFT), including the 2D planar FFT method (Schwarz and et al., 1990), the 2D spherical FFT method (Strang van Hees, 1990), the multi-band 2D spherical FFT approach (Forsberg and Sideris, 1993) and the 1D spherical FFT method (Haagmans and et al., 1992), are presented. The advantages and disadvantages of these approaches are discussed, as well.

2.1 Stokes Integral

The Stokes integral for computing the geoid undulation at an arbitrary point on the geoid can be expressed as (Heiskanen and Moritz, 1967)

$$N = \frac{R}{4\pi\gamma} \iint_{\sigma} \Delta g \; S(\psi) \; d\sigma \, , \tag{1}$$

where R is the mean earth radius, γ the normal gravity, σ the sphere of integration, Δg the gravity anomalies reduced to the geoid, and $S(\psi)$ the Stokes function. To get the true value of the geoidal undulation, the integration should be extended to the whole sphere. For local or regional geoid computation, usually a global geopotential model (GM) is combined with the discrete local gravity data as well as height data. The geopotential model provides the low frequency or long wavelength part of the geoid. Local gravity anomaly data and height data provide the medium and high frequency components of the geoid spectrum. The formula for practical computation of the local geoid by the remove-restore technique is

$$N = N_{GM} + N_{\Delta g} + N_{ind} \, , \tag{2}$$

where N_{GM} is the geoidal undulation implied by the geopotential model, $N_{\Delta g}$ is the contribution of the terrain-corrected mean free air gravity anomalies reduced to the reference field and N_{ind} is the indirect effect of the terrain reduction. The contribution of the GM coefficients can be computed by the spherical harmonic expansion formulas (Heiskanen and Moritz, 1967) given below in spherical approximation for the OSU91A model

$$\Delta g_{GM} = G\sum_{n=2}^{360}(n-1)\sum_{m=0}^{n}[C_{nm}\cos m\lambda + S_{nm}\sin m\lambda]P_{nm}(\sin\varphi), \qquad (3)$$

$$N_{GM} = R\sum_{n=2}^{360}\sum_{m=0}^{n}[C_{nm}\cos m\lambda + S_{nm}\sin m\lambda]P_{nm}(\sin\varphi), \qquad (4)$$

where G is the mean gravity of the earth, C_{nm} and S_{nm} are the fully normalized harmonic coefficients, and P_{nm} are the fully normalized associated Legendre functions.

Given an M x N equi-angular mean gravity anomaly data grid on the sphere, the second term in (2) can be evaluated by (Strang Van Hees, 1990; Haagmans and et al., 1992)

$$N(\varphi_P,\lambda_P) = \frac{R\cdot\Delta\varphi\cdot\Delta\lambda}{4\pi\gamma}\sum_{\varphi_Q=\varphi_1}^{\varphi_M}\sum_{\lambda_Q=\lambda_1}^{\lambda_N} S(\psi_{PQ})\ \Delta g(\varphi_Q,\lambda_Q)\ \cos\varphi_Q\ , \qquad (5)$$

where P, Q denote the computation point and data point respectively, $\Delta\varphi$, $\Delta\lambda$ are the grid spacings in latitude and longitude, M and N are the number of parallels and meridians in the grid, ψ denotes the spherical distance between two points on the sphere, and $S(\psi_{PQ})$ is the Stokes' kernel function computed by

$$S(\psi) = \frac{1}{\sin\frac{\psi}{2}} - 4 - 6\sin\frac{\psi}{2} + 10\sin^2(\frac{\psi}{2}) - [3 - 6\sin^2(\frac{\psi}{2})]\ln[\sin\frac{\psi}{2} + \sin^2(\frac{\psi}{2})]\ , \qquad (6)$$

where

$$\sin^2(\frac{\psi_{PQ}}{2}) = \sin^2(\frac{\Delta\varphi_{PQ}}{2}) + \sin^2(\frac{\Delta\lambda_{PQ}}{2})\cos\varphi_P\cos\varphi_Q \ ,$$

$$\Delta\varphi_{PQ} = \varphi_P - \varphi_Q \ , \qquad \Delta\lambda_{PQ} = \lambda_P - \lambda_Q \ . \tag{7}$$

Δg in formula (5) is the residual mean free-air gravity anomaly which, using Helmert's second condensation reduction, is obtained by

$$\Delta g = \Delta g_{FA} + c + \delta\Delta g - \Delta g_{GM} \ , \tag{8}$$

where the first term on the right hand side of (8) is the mean free air gravity anomaly corrected for atmospheric attraction, the second term c is the classical terrain correction, given in linear approximation by (Sideris, 1984)

$$c = \frac{1}{2}k\ [\iint_E \frac{\rho h^2}{s^3}dxdy - 2h_P \iint_E \frac{\rho h}{s^3}dxdy + h_P^2 \iint_E \frac{\rho}{s^3}dxdy] \ , \tag{9}$$

where ρ is the density of the topographical masses, s is the planar distance between the computation point and data point, and k is Newton's gravitational constant. The third term in equation (8) is the indirect effect on gravity which is very small (smaller than 1 mGal) and can usually be neglected, the fourth term is the reference anomaly computed by the GM coefficients. The indirect effect of Helmert's condensation reduction on the geoid, considering the first two terms in planar approximation, is approximately (Wichiencharoen, 1982)

$$N_{ind} = -\frac{\pi k \rho}{\gamma} h_P^2 - \frac{\pi k \rho}{6\gamma} \iint_E \frac{h^3 - h_P^3}{s^3} dxdy \ . \tag{10}$$

The effects of terrain on the geoid (direct effects) can be directly evaluated by (Sideris et al., 1989)

$$N_d = N_0 + N_1, \tag{11}$$

where N_d denotes the direct effect, N_0, N_1 are the first two terms given by

$$N_0 = -\frac{k\rho}{\gamma}\left[\iint_E \frac{h}{s}\,dxdy - 2h_P \iint_E \frac{1}{s}\,dxdy\right], \tag{12}$$

$$N_1 = -\frac{k\rho}{6\gamma}\left[\iint_E \frac{h^3}{s^3}\,dxdy - 3h_P \iint_E \frac{h^2}{s^3}\,dxdy + 3h_P^2 \iint_E \frac{h}{s^3}\,dxdy + h_P^3 \iint_E \frac{1}{s^3}\,dxdy\right]. \tag{13}$$

Formulae (2) to (10) are the practical formulas widely used for local and regional geoid determination. They have been adopted in this research.

2.2 The 1D and 2D Fourier Transform and Its Properties

The fast Fourier transform is a powerful tool for signal analysis and synthesis in science and engineering. In addition, it can be used to compute the convolution integrals defined in the space or time domain very efficiently in the frequency domain. Since many of the integrals in physical geodesy, including the formulas for geoid computation discussed in the previous section, are themselves convolution integrals and become discrete convolutions on regular grids, they can be evaluated by FFT much faster than the conventional method of pointwise direct summation, generating results on all the grid points in one run. Therefore, the fast Fourier transform has now become a standard procedure for evaluating the discrete integrals in physical geodesy. In the sequel, the definitions of 1D and 2D Fourier transforms are outlined and some of their properties, which are important for their applications in the evaluation of the discrete convolutions encountered in physical geodesy, are outlined.

2.2.1 The 1D and 2D Continuous Fourier Transform (CFT)

The 1D Fourier transform or spectrum of a function h(x) in the space domain is defined (Bracewell, 1986; Brigham, 1988) as

$$H(u) = \int_{-\infty}^{+\infty} h(x)\ e^{-j2\pi ux}\ dx \ = \ \mathbf{F}\,[h(x)]\ , \tag{14}$$

where x is the distance variable, u is the spatial frequency in cycles per distance unit, j is the imaginary unit, and **F** is the direct Fourier transform operator.

Integral (14) gives the spectrum of a function defined in the space domain if the function is known. If the spectrum of a function is known in the frequency domain, the function can be recovered in the time domain by the following inverse Fourier transform:

$$h(x) = \int_{-\infty}^{+\infty} H(u)\ e^{j2\pi ux}\ du \ = \ \mathbf{F}^{-1}\,[H(u)]\ , \tag{15}$$

where $\mathbf{F}^{-1}$ denotes the inverse Fourier transform operator. The Fourier transform pair h(x) and H(u) is denoted as

$$h(x) \leftrightarrow H(u) \,. \tag{16}$$

where $\leftrightarrow$ indicates the Fourier transform pair. Similar to the definition of the above 1D continuous Fourier transform, the 2D continuous Fourier transform of a function h(x,y) can be defined as

$$H(u,v) = \int_{-\infty}^{+\infty}\int_{-\infty}^{+\infty} h(x,y)\; e^{-j2\pi(ux+vy)}\; dx\; dy = \mathbf{F}\,[h(x,y)] \,. \tag{17}$$

The inverse transform is

$$h(x,y) = \int_{-\infty}^{+\infty}\int_{-\infty}^{+\infty} H(u,v)\; e^{-j2\pi(ux+vy)}\; du\; dv = \mathbf{F}^{-1}\,[H(u,v)] \,. \tag{18}$$

The Fourier transform pair is denoted by

$$h(x,y) \leftrightarrow H(u,v) \,. \tag{19}$$

Comparing (17), (18) with (14), (15), one can see that the 2D Fourier transform can be obtained by applying the 1D Fourier transform twice, where each time one of the two variables is held constant.

2.2.2 The 1D and 2D Discrete Fourier Transform (DFT)

In practice, data are usually given on discrete random points for a limited space area. In the one dimensional case, assuming that data are given at M data points with equal spacing Δx, i.e.,

$$x = k\Delta x \ , k=0,1,2,\ldots,M-1 \ , \tag{20}$$

and if X denotes the data length (period), then the data spacing Δx is given by

$$\Delta x = \frac{X}{M} . \tag{21}$$

The 1D discrete Fourier transform of the data sequence is given by

$$H(m\Delta u) = \Delta x \sum_{k=0}^{M-1} h(k\Delta x) \ e^{-j2\pi m\Delta u k\Delta x} \quad , \tag{22}$$

where Δu is the frequency interval given by

$$\Delta u = \frac{1}{X} . \tag{23}$$

From (21) and (23) we have

$$\Delta u\Delta x = \frac{1}{M} \tag{24}$$

Considering (24) we can rewrite (22) as

$$H(m\Delta u) = \Delta x \sum_{k=0}^{M-1} h(k\Delta x)\ e^{-j2\pi\frac{mk}{M}} \tag{25}$$

with m=0,1,2,...,M-1.

The inverse Fourier transform corresponding to (25) is given by

$$\begin{aligned} h(k\Delta x) &= \Delta u \sum_{m=0}^{M-1} H(m\Delta u)\ e^{\,j2\pi\frac{mk}{M}} \\ &= \frac{1}{M\Delta x} \sum_{m=0}^{M-1} H(m\Delta u)\ e^{\,j2\pi\frac{mk}{M}} \end{aligned} \tag{26}$$

with k=0,1,2,..., M.

Similarly, the 2D discrete Fourier transform pair can be defined as

$$H(m\Delta u,\ n\Delta v) = \Delta x\ \Delta y \sum_{k=0}^{M-1} \sum_{l=0}^{N-1} h(k\Delta x,\ l\Delta y)\ e^{-2\pi j(\frac{mk}{M}+\frac{nl}{N})}, \tag{27}$$

$$\begin{aligned} h(k\Delta x,\ l\Delta y) &= \Delta u\ \Delta v \sum_{m=0}^{M-1} \sum_{n=0}^{N-1} H(m\Delta x,\ n\Delta y)\, e^{2\pi j(\frac{mk}{M}+\frac{nl}{N})} \\ &= \frac{1}{M\Delta x}\frac{1}{N\Delta y} \sum_{m=0}^{M-1} \sum_{n=0}^{N-1} H(m\Delta x,\ n\Delta y) e^{2\pi j(\frac{mk}{M}+\frac{nl}{N})}. \end{aligned} \tag{28}$$

The above discrete Fourier transform pair is denoted as

$$h(k,l) \leftrightarrow H(m,n) \ . \tag{29}$$

The discrete Fourier transform can be calculated very efficiently by the fast Fourier transform algorithm. Detailed discussion of the algorithm can be found in many references such as (Brigham, 1988).

2.2.3 Convolution Theorem

One of the most important properties of the Fourier transform is the convolution theorem which allows for evaluation of convolution integrals defined in the space or time domain in the frequency domain with the very efficient FFT algorithm. The 1D and 2D continuous convolution integrals are defined as

$$h(x)*g(x) = \int_{-\infty}^{+\infty} h(x_Q)\ g(x_Q - x)\ dx_Q = g(x)*h(x) \ , \tag{30}$$

$$\begin{aligned} h(x,y)*g(x,y) &= \int_{-\infty}^{+\infty}\int_{-\infty}^{+\infty} h(x_Q,\ y_Q)\ g(x_Q - x,\ y_Q - y)\ dx_Q\ dy_Q \\ &= g(x,y)*h(x,y) \ , \end{aligned} \tag{31}$$

where $*$ denotes convolution. The convolution theorem states that (Brigham,1988; Bracewell, 1986)

$$h(x)*g(x) \leftrightarrow H(u)\ G(u)\ , \tag{32}$$

$$h(x,y)*g(x,y) \leftrightarrow H(u,v)\ G(u,v)\ . \tag{33}$$

The theorem shows that the convolution integral in the space or time domain can be replaced by the product of their spectrum in the frequency domain, i.e., the convolution integral in the space domain can be evaluated by

$$h(x,y)*g(x,y) = \mathbf{F}^{-1}\ [\ \mathbf{F}\ [h(x,y)]\ \mathbf{F}\ [g(x,y)]\ ] \tag{34}$$

or

$$h(x,y)*g(x,y) = \mathbf{F}^{-1}\ [H(u,v)\ G(u,v)]\ . \tag{35}$$

In the discrete case, the corresponding discrete convolutions are defined as

$$h(k)*g(k) = \Delta x \sum_{i=0}^{M-1} h(i)\ g(k-i) \tag{36}$$

$$h(k,l)*g(k,l) = \Delta x \Delta y \sum_{i=0}^{M-1} \sum_{j=0}^{N-1} h(i,j)\ g(k-i,l-j)\ . \tag{37}$$

The convolution theorem in this case has the following form

$$h(k)*g(k) \leftrightarrow H(m)\ G(m)\ , \tag{38}$$

$$h(k,l)*g(k,l) \leftrightarrow H(m,n)\ G(m,n)\ . \tag{39}$$

According to the theorem, the discrete convolution summations specified by (36), (37) can be evaluated by FFT very efficiently in the frequency domain similar to (35), (39) as

$$h(k)*g(k) = \mathbf{F}^{-1} [\ H(m)\ G(m)\ ], \tag{40}$$

$$h(k,l)*g(k,l) = \mathbf{F}^{-1} [\ H(m,n)\ G(m,n)\ ]. \tag{41}$$

As will be shown later, the integrals for terrain correction, direct and indirect effects of the terrain reductions on the geoid, the planar approximation of the Stokes integral and the spherical approximation of the Stokes integral are all 2D discrete convolutions on a given 2D grid and can thus be evaluated by FFT for all the grid points in one run instead of the time-consumming pointwise summation. Even the discretized Stokes integral can be expressed as the linear combination of 1D discrete convolutions and thus be evaluated efficiently by FFT without any approximation.

2.2.4 Some Properties of the Discrete Fourier Transform

In the following, several properties of the discrete Fourier transform which are important for this research are outlined. Detailed discussion and derivation of the properties of the Fourier transform can be found in a number of books, such as (Brigham, 1988) and (Bracewell, 1986). The relation between the 2D discrete convolution and the 1D discrete convolution, which allows for evaluation of the 2D discrete convolution by 1D FFT, are discussed in some detail.

According to (Brigham, 1988), we have the following properties:

(i) Addition theorem (linearity):

$$ah(k,l)+bg(k,l) \leftrightarrow aH(m,n)+bG(m,n), \tag{42}$$

where a,b are constants.

(ii) Shifting theorem:

$$h(k-\lambda,\ l-\mu) \leftrightarrow H(m,n)\ e^{-j2\pi\left(\frac{m\lambda}{M}+\frac{n\mu}{N}\right)}, \tag{43}$$

where λ, μ are integer numbers. Since the origin of the 2D data grid is usually selected at the centre of the grid while some of the FFT subroutines, such as the IMSL subroutine used in this research, assume the south-west corner of the grid as the origin, the shift theorem allows for getting the correct spectrum of the data grid by using these subroutines.

By rewritting the 2D discrete convolution summation (37) as

$$h(k,l)*g(k,l) = \Delta x \sum_{i=0}^{M-1} \{\ \Delta y \sum_{j=0}^{N-1} h(i,j)\ g(k-i,l-j)\ \} \tag{44}$$

we can see that the summation in the brackets of (44) is actually a 1D discrete convolution summation for fixed k and can be evaluated by the 1D FFT. By applying the addition theorem (42) to (44) one gets

$$
\begin{aligned}
h(k,l)*g(k,l) &= \Delta x \sum_{i=0}^{M-1} \mathbf{F}^{-1}\{\ \mathbf{F}[h(i,j)]\ \mathbf{F}\ [g(k,l)\ ]\ \} \\
&= \mathbf{F}^{-1}\ \{\Delta x \sum_{i=0}^{M-1} \{\ \mathbf{F}[h(i,j)]\ \ \mathbf{F}[g(k,l)\ ]\ \}\ \}
\end{aligned}
\tag{45}
$$

for fixed k.

The major advantage of computing the 2D discrete convolution by 1D FFT through (45) is that the computer memory required is reduced dramatically, which is especially important for dealing with large 2D data sets on small computers or microcomputers, as is the case with the computation of large scale continental geoid in this research. Another advantage is that it is possible to reformulate the 2D discrete Stokes integral, which is not a 2D discrete convolution by itself, in such a way that it can be evaluated rigorously parallel by parallel by the 1D FFT method (Haagmans and et al., 1992).

2.3 The FFT-Based Methods For Evaluating The Discrete Stokes Integral

In principle, the residual part of the geoid undulation at each grid point can be obtained by direct evaluation of the discrete summation (5) of the Stokes integral. But the summation has to be repeated for every point. For the computation of large-scale regional geoids, such as the current Canadian geoid with a 660x1320 grid, the computational burden is too big to be handled efficiently, even on medium-size or large computers, needless to say microcomputers. Therefore, the FFT-based numerical methods which allow for a fast evaluation of discrete convolutions using all the data on the grid are the only realistic approach to the problem. Currently, three FFT-based techniques are available for the evaluation of the discrete Stokes integral and have been included in the PC-based software package in this research. They will be briefly described in the following three subsections.

2.3.1 The 2D Planar FFT Formulas

In planar approximation, the discrete Stokes formula (5) becomes (Schwarz and et al., 1990)

$$N(x_P,y_P)=\frac{\Delta x\cdot\Delta y}{2\pi\gamma}\sum_{x_Q=x_1}^{x_M}\sum_{y_Q=y_1}^{y_N}\frac{1}{l_{PQ}}\,\Delta g(x_Q,y_Q)\,, \tag{46}$$

where l_{PQ} is the horizontal distance between points P and Q, and Δx, Δy are the grid spacings in x and y directions. Equation (46) is a 2D discrete convolution and can be evaluated by 2D FFT (Schwarz and et al., 1990)

$$N(x_P,y_P)=\frac{\Delta x\Delta y}{2\pi\gamma}\;\mathbf{F}^{-1}\,[\,\mathbf{F}[\frac{1}{l_P}]\,\mathbf{F}(\Delta g_P]\,]\,. \tag{47}$$

With appropriate zero padding of the gridded data, the 2D FFT algorithm of eq.(47) will give the same results as those obtained by direct evaluation of (46) for all the grid points in one run. Thus, the original discrete Stokes integral is approximated by summation (46) on the plane which can be evaluated by 2D FFT enhancing the computational efficiency dramatically. The sacrifice is the loss of accuracy due to planar approximation. As will be shown later in the numerical results, the loss of accuracy is significant mainly in mountainous area with rough topography but negligible in flat area when a high degree geopotential model is combined with the local data.

The 2D discrete convolution (46) can also be evaluated through 1D FFT in the same way as discussed in 2.2.4. By applying (45) we have

$$N(x_P, y_P) = \frac{\Delta x \cdot \Delta y}{2\pi\gamma} \; \mathbf{F}^{-1} \Big[\sum_{x_P = x_1}^{x_M} \; \mathbf{F} \, [\frac{1}{l_P}] \; \mathbf{F} \, [\Delta g(x_P, y_P] \Big] \tag{48}$$

with fixed x_P, or equivalently

$$N(x_P, y_P) = \frac{\Delta x \cdot \Delta y}{2\pi\gamma} \; \mathbf{F}^{-1} \Big[\sum_{y_P = y_1}^{y_M} \; \mathbf{F} \, [\frac{1}{l_P}] \; \mathbf{F} \, [\Delta g(x_P, y_P] \Big] \tag{49}$$

with y_P fixed. (48) or (49) are used in the case where the grid size is too large to be handled by the capacity of the available computer memory.

2.3.2 The 2D Spherical FFT Formula

In planar approximation, the true Stokes kernel function as specified by equations (6) and (7) is approximated for small distance ψ by

$$S(\psi_{PQ}) \approx \frac{1}{\sin\frac{\psi_{PQ}}{2}} \approx \frac{2}{\psi_{PQ}} \approx \frac{2R}{l_{PQ}} . \tag{50}$$

The effect of the approximation on the geoid will increase with the area of integration although this error can be reduced by adopting a higher order geopotential model. To overcome this limitation, Strang van Hees (1990) put forward an approach to approximate the true Stokes function directly on the sphere by means of spherical trigonometry. As can be seen from equations (6) and (7), Stokes function is not only a function of latitude and longitude differences but also a function of the latitudes of both the computation point P and the data point Q. Therefore, the discrete Stokes integral (eq.(5)) is not a 2D discrete convolution and can not be evaluated by 2D FFT. In Strang van Hees' approach, Stokes' function is still computed by eq.(6). But the term involving $\cos\varphi_p\cos\varphi_q$ in eq.(7) is approximated by

$$\cos\varphi_P \cos\varphi_Q \approx \cos^2\varphi_m - \sin^2\frac{1}{2}(\varphi_P - \varphi_Q) , \tag{51}$$

where φ_m is the mean latitude of the whole integration area. Thus the approximated Stokes function is only dependent on the latitude and longitude difference. Equation (5) becomes a 2D discrete convolution and can be efficiently evaluated by 2D FFT on the sphere. The formula is (Strang Van Hees, 1990; Forsberg and Sideris, 1993)

$$N(\varphi_P,\lambda_P) = \frac{R\cdot\Delta\varphi\cdot\Delta\lambda}{4\pi\gamma}\ \mathbf{F}^{-1}\ [\ \mathbf{F}[S(\psi_P]\ \mathbf{F}[\Delta g(\varphi_P,\lambda_P)\ \cos\varphi_P\ ]\ ] . \tag{52}$$

This approach avoids the limitation of planar FFT but introduces a latitude-dependent error to the computed geoid. Only the grid points located on the parallel with the mean latitude φ_m are free from this error (equation (51) strictly holds only on this parallel). This approach was adopted for the computation of the American continental geoid, GEOID90 (Milbert, 1990), and was also used to compute a geoid file for the area of Canada in this research.

2.3.3 The Multi-Band Spherical FFT Approach

As mentioned above, the 2D spherical FFT formula is subject to a latitude-dependent error which is not negligible for the determination of large scale regional geoids. On the other hand, the approach gives exactly the same results as the direct summation using the true discrete Stokes integration for the points on the parallel with the mean latitude. This property was employed by Forsberg and Sideris (1993) to propose a so-called multi-band spherical FFT approach which reduces the latitude-dependent error inherent in Strang Van Hees' approach. In this approach, the whole area is divided into a set of latitude bands extending from north to south. For the i-th band, the geoidal undulations at all the points in the band are obtained still by Strang van Hees' 2D spherical FFT method (see eq.(52)) while using the mean latitude φ_i for computing Stokes' kernel function for all points in the band. If the i-th computation makes use of all the data on the whole grid (this means that one has to perform a 2D FFT for the whole grid at the i-th computation), then the computed undulations at all the points along the i-th parallel will be exactly the same as those obtained by direct integration using (5) for all the data grid points. Obviously, if the whole area is divided into n zones, the computation time will be about n times that of usuall 2D spherical

FFT to get the exact solution. The alternative is to perform 2D FFT only within a certain band with some overlappings between neighbouring zones, at the price of losing some accuracy due to discarding the data outside each zone. The geoidal undulations at points between two neighbouring overlapping zones can be obtained by linear interpolation (Forsberg and Sideris, 1993), namely

$$N(\varphi) = \frac{\varphi - \varphi_{i+1}}{\varphi_i - \varphi_{i+1}} N_i + \frac{\varphi_{i+1} - \varphi}{\varphi_i - \varphi_{i+1}} N_{i+1}, \tag{53}$$

where N_i, N_{i+1} are the undulations at the point from two neighbouring computations.

2.3.4 The 1D Spherical FFT Formula

To overcome the limitations of the previous 2D FFT methods, Haagmans and et al. (1992) made further use of the property that Strang van Hees' 2D FFT gives the exact undulations for all the points along the parallel of mean latitude. Using this property and the addition theorem of FFT, he came up with an approach which allows for the evaluation of the true discrete Stokes integral without approximation, parallel by parallel, by means of the 1D FFT. In fact, for fixed latitude φ_p on a certain parallel, the summation in the longitude direction in the 2D discrete Stokes integral (5) is a one dimensional discrete convolution and can be evaluated by 1D FFT. By employing the addition theorem of DFT (see equation. (42)), the discrete Stokes integral (5) for the fixed parallel can be evaluated by (Haagmans and et al., 1992)

$$N(\varphi_P,\lambda_P)=\frac{R\cdot\Delta\varphi\cdot\Delta\lambda}{4\pi\gamma}\,\mathbf{F}^{-1}\left[\sum_{\varphi_P=\varphi_1}^{\varphi_M}\mathbf{F}[S(\psi_P)]\;\mathbf{F}\left[\Delta g(\varphi_P,\lambda_P)\cos\varphi_P\right]\right] \tag{54}$$

with φ_P fixed. Eq. (54) yields the geoidal heights for all the points on one parallel which are strictly equivalent to those obtained by direct summation using (5) point by point.

The major advantage of the 1D spherical FFT approach is that it gives exactly the same results as those obtained by direct numerical integration. In addition, it only needs to deal with one 1D complex array each time, resulting in a considerable saving in computer memory as compared to the 2D FFT techniques discussed before. In fact, assuming that the grid size is 660x1320 (the same size as the Canadian geoid to be computed), the memory required for storing the two 1320x2640 complex 2D arrays (after zero padding the grid is extended 4 times as large as the original grid) when the 2D FFT methods are used will be 55.7 MB and 111.4 MB for single precision and double precision, respectively, while the 1D FFT technique only needs one one-dimensional complex array of the size of 2640 elements occupying a memory of only 0.42 MB for storing the spectrum of the undulations for each parallel. Moreover, the adoption of FFT makes it far more efficient computationally than the classical direct numerical integration. Detailed comparisons of various techniques can be found in (Haagmans and et al., 1992; Forsberg and Sideris, 1993).

2.5 The 2D and 1D FFT Formulae for Terrain Corrections, and Direct and Indirect Topographic Effects

Given a MxN digital height grid on the plane, the indirect effect of the Helmert's condensation reduction is computed by the following discrete integral corresponding to (10)

$$N_{ind_P} = -\frac{\pi k \rho}{\gamma} h_P^2 + \frac{\pi k \rho \Delta x \Delta y}{6\gamma} h_P^3 \sum_{x_Q=x_1}^{x_M} \sum_{y_Q=y_1}^{y_N} \frac{1}{l_{PQ}} - \frac{\pi k \rho \Delta x \Delta y}{3\gamma} \sum_{x_Q=x_1}^{x_M} \sum_{y_Q=y_1}^{y_N} \frac{1}{l_{PQ}} h_Q^3 \ . \tag{55}$$

Obviously, the second term and the third term on the right-hand side of (55) are two 2D discrete convolutions and can be evaluated by 2D FFT efficiently, yielding the indirect effects for all the grid points in one run. Since the summations in both the x and the y direction are 1D convolutions, (55) can also be evaluated by 1D FFT either row by row or column by column. The 1D and 2D FFT formulas for evaluating (55) are as follows

$$\begin{aligned} N_{ind_P} = & -\frac{\pi k \rho}{\gamma} h_P^2 + \frac{\pi k \rho \Delta x \Delta y}{6\gamma} h_P^3 \ \mathbf{F}^{-1} \left[\sum_{x_P=x_1}^{x_M} \mathbf{F}[\frac{1}{l_P}] \ \mathbf{F}[1] \right] \\ & - \frac{\pi k \rho \Delta x \Delta y}{6\gamma} \ \mathbf{F}^{-1} \left[\sum_{x_P=x_1}^{x_M} \mathbf{F}[\frac{1}{l_P}] \ \mathbf{F}\,[h_P^3] \right] , \end{aligned} \tag{56}$$

$$\begin{aligned} N_{ind_P} = & -\frac{\pi k \rho}{\gamma} h_P^2 + \frac{\pi k \rho \Delta x \Delta y}{6\gamma} h_P^3 \ \mathbf{F}^{-1} \left[\mathbf{F}\,[\frac{1}{l_P}] \ \mathbf{F}[1] \right] \\ & - \frac{\pi k \rho \Delta x \Delta y}{6\gamma} \ \mathbf{F}^{-1} \left[\mathbf{F}[\frac{1}{l_P}] \ \mathbf{F}[h_P^3] \right] \end{aligned} \tag{57}$$

Equation (56) is the 1D FFT equation for evaluating indirect effects row by row. The formula for evaluating the indirect effects column by column can be written as

$$N_{ind_P} = -\frac{\pi k\rho}{\gamma} h_P^2 + \frac{\pi k\rho\Delta x\Delta y}{6\gamma} h_P^3 \; F^{-1} [\sum_{y_P=y_1}^{y_M} F[\frac{1}{l_P}] \; F[1]]$$
$$-\frac{\pi k\rho\Delta x\Delta y}{6\gamma} \; F^{-1} [\sum_{y_P=x_1}^{y_M} F[\frac{1}{l_P}] \; F\,[h_P^3]] \,. \tag{58}$$

Discretizing integral (9) for terrain correction and integrals (12), (13) for direct effects, we have the corresponding 2D discrete convolution summations

$$c_P = \frac{k\rho\Delta x\Delta y}{2} \{ \sum_{x_Q=x_1}^{x_M} \sum_{y_Q=y_1}^{y_N} \frac{h_Q^2}{l_{PQ}^3} - 2h_P \sum_{x_Q=x_1}^{x_M} \sum_{y_Q=y_1}^{y_N} \frac{1}{l_{PQ}^3} h_Q$$
$$+ h_P^2 \sum_{x_Q=x1}^{x_M} \sum_{y_Q=y_1}^{y_N} \frac{1}{l_{PQ}^3} \}, \tag{59}$$

$$N_{0_P} = -\frac{k\rho\Delta x\Delta y}{\gamma} \{ \sum_{x_Q=x_1}^{x_M} \sum_{y_Q=y_1}^{y_N} \frac{h_Q}{l_{PQ}} - 2h_P \sum_{x_Q=x_1}^{x_M} \sum_{y_Q=y_1}^{y_N} \frac{1}{l_{PQ}} \}, \tag{60}$$

$$N_{1P} = -\frac{k\rho\Delta x\Delta y}{6\gamma}\{\sum_{x_Q=x_1}^{x_M}\sum_{y_Q=y_1}^{y_N}\frac{h_Q^3}{l_{PQ}^3} - 3h_P\sum_{x_Q=x_1}^{x_M}\sum_{y_Q=y_1}^{y_N}\frac{h_Q^2}{l_{PQ}^3}$$

$$+ 3h_P^2\sum_{x_Q=x_1}^{x_M}\sum_{y_Q=y_1}^{y_N}\frac{h_Q}{l_{PQ}^3} + h_P^3\sum_{x_Q=x_1}^{x_M}\sum_{y_Q=y_1}^{y_N}\frac{h_Q^3}{l_{PQ}^3}\}. \tag{61}$$

The 2D FFT formulas for evaluating (59), (60) and (61) are

$$C_P = \frac{k\rho\Delta x\Delta y}{2}\{\mathbf{F}^{-1}[\mathbf{F}[\frac{1}{l_P^3}]\mathbf{F}[h_P^2]] - 2h_P\mathbf{F}^{-1}[\mathbf{F}[\frac{1}{l_P^3}]\mathbf{F}[h_P]]$$

$$+ h_P^2\mathbf{F}^{-1}[\mathbf{F}[\frac{1}{l_P^3}]\mathbf{F}[1]]\}, \tag{62}$$

$$N_{0P} = -\frac{k\rho\Delta x\Delta y}{\gamma}\{\mathbf{F}^{-1}[\mathbf{F}[\frac{1}{l_P}]\mathbf{F}[h_P]] - 2h_P\mathbf{F}^{-1}[\mathbf{F}[\frac{1}{l_P}]\mathbf{F}[1]]\}, \tag{63}$$

$$N_{1P} = -\frac{k\rho\Delta x\Delta y}{6\gamma}\{\mathbf{F}^{-1}[\mathbf{F}[\frac{1}{l_P^3}]\mathbf{F}[h_P^3]] - 3h_P\mathbf{F}^{-1}[\mathbf{F}[\frac{1}{l_P^3}]\mathbf{F}[h_P^2]]$$

$$+ 3h_P^2\mathbf{F}^{-1}[\mathbf{F}[\frac{1}{l_P^3}]\mathbf{F}[h_P]] + h_P^3\mathbf{F}^{-1}[\mathbf{F}[\frac{1}{l_P^3}]\mathbf{F}[1]]\}. \tag{64}$$

The 2D discrete convolutions (59), (60), (61) can also be evaluated by 1D FFT row by row using the following formulas:

$$C_P = \frac{k\rho\Delta x\Delta y}{2}\{ \mathbf{F}^{-1}[\sum_{x_P=x_1}^{x_M} \mathbf{F}[\frac{1}{l_P^3}]\, \mathbf{F}[h_P^2]]$$

$$-2h_P\ \mathbf{F}^{-1}[\sum_{x_P=x_1}^{x_M} \mathbf{F}[\frac{1}{l_P^3}]\, \mathbf{F}[h_P] \} \tag{65}$$

$$+ h_P^2\ \mathbf{F}^{-1}[\sum_{x_P=x_1}^{x_M} \mathbf{F}[\frac{1}{l_P^3}]\, \mathbf{F}[1]] \} ,$$

$$N_{0_P} = -\frac{k\rho\Delta x\Delta y}{\gamma}\{ \mathbf{F}^{-1}[\sum_{x_P=x_1}^{x_M} \mathbf{F}[\frac{1}{l_P}]\, \mathbf{F}[h_P]]$$

$$-2h_P\ \mathbf{F}^{-1}[\sum_{x_P=x_1}^{x_M} \mathbf{F}[\frac{1}{l_P}]\, \mathbf{F}[1]] \} , \tag{66}$$

$$N_{1_P} = -\frac{k\rho\Delta x\Delta y}{6\gamma}\{ \mathbf{F}^{-1}[\sum_{x_P=x_1}^{x_M} \mathbf{F}[\frac{1}{l_P^3}]\, \mathbf{F}[h_P^3]]$$

$$-3h_P\mathbf{F}^{-1}[\sum_{x_P=x_1}^{x_M} \mathbf{F}[\frac{1}{l_P^3}]\, \mathbf{F}[h_P^2]]$$

$$+ 3h_P^2\mathbf{F}^{-1}[\sum_{x_P=x_1}^{x_M} \mathbf{F}[\frac{1}{l_P^3}]\, \mathbf{F}[h_P]] \tag{67}$$

$$+ 3h_P^2\mathbf{F}^{-1}[\sum_{x_P=x_1}^{x_M} \mathbf{F}[\frac{1}{l_P^3}]\, \mathbf{F}[1]] \}$$

with x_P fixed. If y_P is fixed, the evaluation can be done column by colum using

$$C_P = \frac{k\rho\Delta x\Delta y}{2}\{ F^{-1}[\sum_{y_P=y_1}^{y_M} F [\frac{1}{l_P^3}] F [h_P^2]]$$

$$-2h_P F^{-1}[\sum_{y_P=y_1}^{y_M} F [\frac{1}{l_P^3}] F [h_P] \} \tag{68}$$

$$+ h_P^2 F^{-1}[\sum_{y_P=y_1}^{y_M} F [\frac{1}{l_P^3}] F [1]] \},$$

$$N_{0_P} = -\frac{k\rho\Delta x\Delta y}{\gamma}\{ F^{-1}[\sum_{y_P=y_1}^{y_M} F [\frac{1}{l_P}] F [h_P]]$$

$$-2h_P F^{-1}[\sum_{y_P=y_1}^{y_M} F [\frac{1}{l_P}] F [1]] \} , \tag{69}$$

$$N_{1_P} = -\frac{k\rho\Delta x\Delta y}{6\gamma}\{ F^{-1}[\sum_{y_P=y_1}^{y_M} F [\frac{1}{l_P^3}] F [h_P^3]]$$

$$-3h_P F^{-1}[\sum_{y_P=y_1}^{y_M} F [\frac{1}{l_P^3}] F [h_P^2]]$$

$$+ 3h_P^2 F^{-1}[\sum_{y_P=y_1}^{y_M} F [\frac{1}{l_P^3}] F [h_P]]$$

$$+ 3h_P^2 \mathbf{F}^{-1}[\sum_{y_P=y_1}^{y_M} \mathbf{F} [\frac{1}{l_P^3}] \mathbf{F} [1]] \} . \tag{70}$$

Considering the computational efficiency, one may choose the 1D FFT formulas in the direction with the smaller number of columns or rows. If the number of rows M is smaller than the number of columns, it is computationally more efficient to use the 1D FFT formulas row by row, since the number of direct Fourier transforms required to evaluate each row is less than that column by column. The gain in computational efficiency will be very significant if (M-N) is large.

Whether to adopt the 2D FFT formulas or the 1D FFT formulas depends on the computer memory available. The difference in computer memory requirements is dramatic between the two methods. Taking the evaluation of the direct effect of terrain on the geoid, i.e., eq.(60) and (61), as an example, one has to evaluate six 2D discrete convolutions. Considering the common terms in these convolution summations, we need at least six 2D complex arrays to store the spectrum of data and kernel functions. Since the original data grid has to be extended 50% in all directions for proper zero padding to get the correct results, the size of each array will be 4 MxN. The memory to be allocated to these six arrays will be 192 MxN bytes for single precision and 384 MxN bytes for double precision. Assuming that the grid size of the digital terrain model is 1000x1000 (as is the case in B.C.), the memory required will be 192 MB and 384 MB respectively, which is too big to be handled even on large computers, needless to say microcomputers. If one stores the data and intermediate results on hard disk or some other type of external memory device, the read and write operations will make the program extremely slow. However, if one uses the 1D FFT approach, one only needs one MxN real array to store the height grid and twelve 2N or 2M one dimensional complex arrays to perform the computation. In double precision mode, the memory required for these work arrays is less than 5 MB, which most of the microcomputers can handle. In this research, a software package has been written for evaluating the indirect effects, the direct effects, and the terrain correction by the 1D FFT approach on a PC 486 computer.

2.6 Zero Padding for Eliminating the Effects of Cyclic Convolution

When applying the FFT formulae described above directly to the original data grid, the results will not be equal to those obtained by the direct evaluation of the discrete convolutions through pointwise summation due to the effect of circular convolution with FFT using data in a limited domain. As will be shown later in the numerical results, the effect of this error can be as large as 24 cm RMS in computing the Canadian geoid. Proper zero padding must be used to overcome this effect (Brigham, 1988). To obtain the same results as those by direct summation, the original data grid (gravity anomaly grid or height grid) should be extended 50% in all directions with zeros and the kernel function should also be extended 50% in all directions with its values (not zeros) (Sideris and Li., 1992 and 1993; Haagmans and et al., 1992). In the case of 1D spherical FFT, one only has to extend the data and kernel functions in longitude direction, resulting in a considerable saving in computer memory. More detailed discussions on the cyclic convolution problem and the ways to deal with it can be found in the above references.

CHAPTER 3

PRECISION OF GEOIDAL UNDULATIONS - ERROR PROPAGATION

In theory, the exact evaluation of the geoidal undulations requires continuous coverage of errorless gravity anomaly data all over the earth. In practice, only discrete noisy gravity anomaly data over limited areas are available. For local geoid determination, usually the local gravity anomaly data are combined with height data and a geopotential model of certain degree and order. Therefore, the accuracy of the geoid obtained using these data depends on the density, coverage and accuracy of the local gravity anomaly and height data, and the errors of the adopted geopotential model. In this research, only the error variances of the gravity anomaly measurements and the noise variances of the geopotential model coefficients (commission error) are available. Therefore, attempts were made to only evaluate their effects upon the precision of the geoidal undulations through error propagation.

In this chapter, the formulas for evaluating the error variances of the computed geoidal undulations due to the gravity anomaly measurement noise are derived by error propagation, which can be evaluated efficiently through 1D spherical FFT. Formulas for computing the effect of the commission error and truncation error of the geopotential coefficients upon the geoid undulations are briefly reviewed, as well.

3.1 Formulas for Error Propagation by FFT

Assuming that the errors of the gravity anomaly data are uncorrelated and their a priori variances are known, then their effect on the computed geoidal height can be derived by error propagation through (5) as

$$\sigma^2_{N_{\Delta g}} = \left(\frac{R\cdot\Delta\varphi\cdot\Delta\lambda}{4\pi\gamma}\right)^2 \sum_{\varphi_Q=\varphi_1}^{\varphi_M} \sum_{\lambda_Q=\lambda_1}^{\lambda_N} (S(\psi_{PQ})\cos\varphi_Q)^2 \sigma^2_{\Delta g(\varphi_Q,\lambda_Q)} \tag{71}$$

where σ^2 denotes the variance. Equation (71) can be evaluated by the 1D FFT as

$$\sigma^2_{N_{\Delta g}} = \left(\frac{R\cdot\Delta\varphi\cdot\Delta\lambda}{4\pi\gamma}\right)^2 F^{-1}\left[\sum_{\varphi_P=\varphi_1}^{\varphi_M} F[(S(\psi_P))^2]\ F[\sigma^2_{\Delta g(\varphi_P,\lambda_P)}\cos^2\varphi_P]\right]. \tag{72}$$

The contribution of the random noise in the GM coefficients (commission error) to the geoidal undulation error variance, neglecting the correlation beween the coefficient errors, can be computed by

$$\sigma^2_{N_{GM}} = R^2 \sum_{n=2}^{N_{max}} \sum_{m=0}^{n} (\sigma^2_{C_{nm}} + \sigma^2_{S_{nm}}), \tag{73}$$

where the two terms in the brackets of (73) are the given variances of the fully normalized geopotential coefficients. Formula (73) gives the global mean variance of the geoidal undulation contributed from the commission error of the geopotential model coefficients. Using the given variances of the OSU91A geopotential model coefficients complete to degree and order 360, (73) gives a standard deviation of about 0.49 m for the point undulation. Table 3.1 (the numerical values in the table are taken from (Rapp and et al., 1991)) gives the geoid undulation commission error by spherical harmonic degree for OSU91A.

Combined with a truncation error of about 24cm (Rapp and et al., 1991), the total point geoidal undulation error is about 54cm for OSU91A complete to degree and order 360. Note that this error is the global mean error and the actual error for different areas may be larger or smaller depending on the data coverage, density, quality, and the roughness of topography. As will be shown later in comparing the model-implied undulations with the GPS/levelling-derived geoidal undulations, the error in Canada is over-estimated for areas with good gravity coverage and mild terrain but under-estimated in mountainous area with rough terrain, such as the area of British Columbia.

By error propagation through (4) we derive the point-dependent formula for evaluating the geoidal undulation commission error as

$$\sigma^2_{N_{GM}} = R^2 \sum_{n=2}^{N_{max}} \sum_{m=0}^{n} [\sigma^2_{C_{nm}} \cos^2 m\lambda + \sigma^2_{S_{nm}} \sin^2 m\lambda] \; P^2_{nm}(\sin\varphi) \; . \qquad (74)$$

Table 3.1 The Commission Error of Point Undulation (Units: cm) For OSU91A (After Rapp et al., 1991)

Degree	By Degree	Cumulative
2	0.2	0.2
6	1.3	2.2
10	2.4	5.0
20	3.6	10.6
30	4.3	16.8
50	3.0	24.8
75	3.7	32.3
100	3.2	36.5
180	2.2	43.2
360	1.3	48.7

When estimating the total undulation error in local geoid determination, the truncation error of the geoidal undulation derived from a geopotential model should not be included due to the introduction of local data of a higher density which allows for resolving the higher frequency part of the geoid spectrum. In fact, according to Schwarz (1984), the low and medium part (from degree 2 to 360) of the gravity spectrum dominates the undulation spectrum.

3.2 The Precision of Relative Undulation

So far, only the point geoidal undulation error has been discussed. In terms of the relative geoidal undulation error, it can also be evaluated in two parts: the contribution of the gravity anomaly data noise and the contribution from the geopotential model coefficient errors. Considering the correlation between undulation errors at any two points, the contribution of the anomaly measurement error to the undulation difference error can be computed simply by

$$\sigma^2_{\Delta N_{PQ}} = \sigma^2_{N_P} + \sigma^2_{N_Q} + \mathrm{cov}(N_P, N_Q) \quad , \tag{75}$$

where the first two terms on the right hand side of (75) are the variances of the undulations at point P and Q to be computed by FFT using (72). The third term is the covariance between the geoidal undulation errors at the two points. Assuming that the gravity anomaly data errors at all grid points are uncorrelated, then the covariance can be derived by error propagation through (5) as

$$\mathrm{cov}(N_P, N_Q) = \left(\frac{R \cdot \Delta\varphi \cdot \Delta\lambda}{4\pi\gamma}\right)^2 \sum_{\varphi_B=\varphi_1}^{\varphi_M} \sum_{\lambda_B=\lambda_1}^{\lambda_N} S(\psi_{PB}) S(\psi_{QB}) \cos^2\varphi_B \quad \sigma^2_{\Delta g(\varphi_B, \lambda_B)}, \tag{76}$$

where B denotes the data point. Unlike eq. (72), the summation in the direction of longitude in eq.(76) is no longer a one dimensional discrete convolution. Therefore, the covariance between the geoidal undulation errors due to the effect of the uncorrelated anomaly data errors can not be computed by the 1D FFT technique on the sphere. It can only be evaluated by direct summation. Neglecting the third term in (75), the relative undulation error standard deviation due to the gravity data noise can be computed approximately by

$$\sigma^2_{\Delta N_{PQ}} = \sigma^2_{N_P} + \sigma^2_{N_Q} \; . \tag{77}$$

The contribution of the geopotential coefficient errors can be evaluated (Christodoulidis, 1976; Rapp and et al., 1991) as follows

Commission error:

$$C^2_{PQ} = \frac{2R^2}{\gamma^2} \sum_{n=2}^{360} \frac{1}{(n-1)^2} \, \varepsilon_n^2 \; s^{n+2} \, [1 - P_n(\cos\psi_{PQ})] \, . \tag{78}$$

Truncation error:

$$T^2_{PQ} = \frac{2R^2}{\gamma^2} \sum_{n=360}^{\infty} \frac{1}{(n-1)^2} \, c_n^2 \; s^{n+2} \, [1 - P_n(\cos\psi_{PQ})] \tag{79}$$

where ε_n and c_n are the error anomaly degree variances and the anomaly degree variances of the geopotential model, s is a scale factor close to 1. Table 3.2 lists the commision error of geoidal undulation differences for OSU91A at different distances (the numerical values are taken from (Rapp and et al., 1991)).

Table 3.2 The Commission Errors of Relative Undulations for OSU91A

Linear Distance (km)	Angular Distance (deg.)	Commission Error (cm)
10	0.09	9.2
20	0.18	18.1
30	0.27	26.6
40	0.36	34.4
50	0.45	41.3
70	0.63	52.4
90	0.81	59.6
100	0.90	62.0
200	1.80	71.8
400	3.60	77.1
600	5.40	77.7
800	7.19	77.7
1000	8.99	77.8
1600	14.39	77.4
2000	17.99	77.4
10000	89.93	77.4

As shown in the table, the relative undulation error of the geopotential model shows a trend of increasing with distances which is further verified by the results of comparing the model-implied geoid with the GPS/levelling derived undulations in chapter 6. Again, the values in table 3.2 are global mean relative errors. For different areas, the error may be larger or smaller. Later, the above commission error of the relative undulations will be combined with the relative error from the contribution of anomaly data noise (equation (77)) to generate the relative error estimates (internal precision) of the geoidal undulation differences for comparison with the results of external precision in chapter 6.

In this chapter, practical formulas for evaluating the effect of the gravity anomaly data noise upon the geoidal undulation variance by FFT were given. Approximate formulas for evaluating the precision of both point and relative undulation were also introduced. These formulas will be used to compute the error variances of the geoidal undulations using the given a priori statistical information of the gravity data and the GM coefficient noise. The internal error estimates thus obtained will be used for comparison with the actual error estimates obtained from comparing the gravimetric geoid with the GPS/levelling-derived geoidal undulations. It will provide useful information on the relation between the data precision and the model errors, and the accuracy of the computed local or regional geoid. This information is important for examining the causes of some large discrepancies of the gravimetric geoid with respect to the GPS/levelling data at some of the stations and for finding appropriate ways to minimize the effects of various errors on the geoid by data combination. It must be mentioned that the formulas discussed in this chapter just give the internal error variances of both point and relative undulation errors under the assumption that the gravity anomaly data noise at different grid points is uncorrelated (only the error variances of the gravity anomaly data are available in this research). If the error covariance function of the gravity anomaly data is known and the error covariance function of geoidal undulations is assumed to be distance-dependent (homogeneous and isotropic), we can get the error covariance function of both point and relative undulations in the form of harmonic expansion. Detailed formulas of this type and their applications can be found in (Sideris and Schwarz, 1986; Strang van Hees, 1986). Various theoretical aspects in error minimization in geoid determination in the space domain and/or frequency domain can be found in (Sjöberg, 1984, 1986, 1991; Yan, 1992; Sideris, 1987; Kearsley, 1984; etc.).

CHAPTER 4

COMPUTER SOFTWARE

To fulfill the objectives of this research project, a PC-based software package has been developed based upon the formulas described in chapter 2 and chapter 3. The package includes the programs described below.

The first program, called N_1DFFT, is the major program which performs the computation of geoidal undulation as well as error propagation by the 1D spherical FFT and/or by direct summation. Due to the adoption of the 1D FFT algorithm, the program can be applied for computing large-scale continental geoids efficiently on microcomputers. The requirement on memory for computing the current Canadian geoid (660x1320 grid) is about 7 MB. The program was designed in such a way that it can compute the geoid for the whole grid or a subgrid of the whole grid or even a few parallels. All computations are controlled by two control parameters for selecting options and methods and an input file containing the grid sizes, spacings, grid boundary limits, I/O data file names and formats of random access I/O data files. Figure 4.1 shows the block diagram of the program.

Figure 4.1 Block Diagram of Program N_1DFFT for Geoid Computation

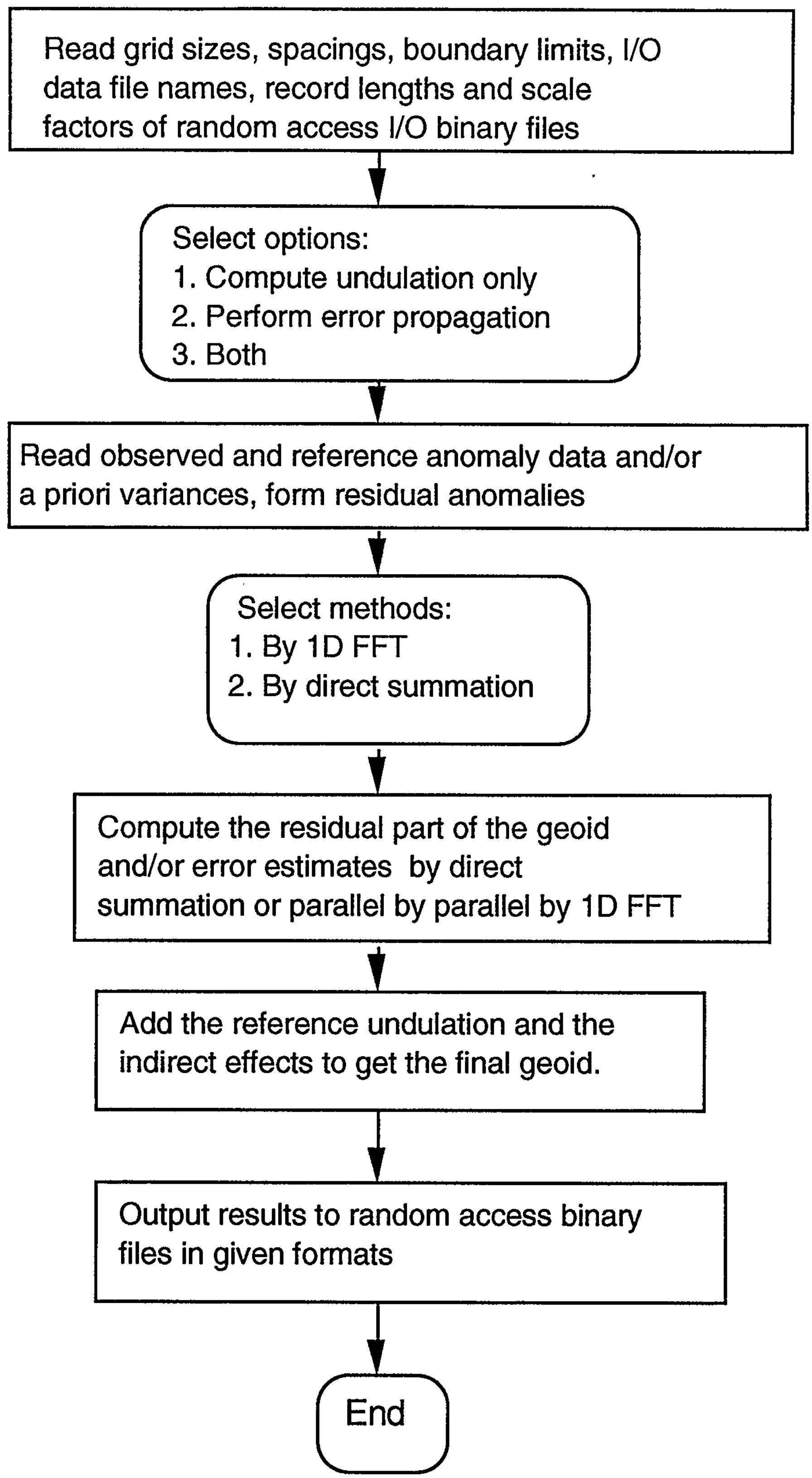

The second program, called N_2DFFT, computes the geoidal undulations by the 2D spherical FFT or by the 2D planar FFT. The third program, called TC_2DFFT, computes the indirect effects of Helmert's second condensation reduction of up to second order by the 2D FFT. The fourth program, called TC_1DFFT, computes the terrain correction, the indirect effect and the direct effect of Helmert's condensation reduction by means of the 1D FFT. It has the option of computing each or all of them.

The above four programs accept direct random access binary files as input and output files to improve the computational efficiency and save memory. All the programs are written in Lahey Fortran 77 and realized on a PC 486/50i computer with 20MB of RAM.

The 5th program, called STAT, performs the comparison between the gravimetric geoid and the GPS/levelling geoid, producing statistics of both absolute and relative agreements of the gravimetric geoid with respect to the GPS/levelling datum. The program also performs datum transformation between the two data sets by regression, removing the systematic datum difference between the two types of undulations.

The 6th program, called PLOTCTR, performs the interpolation as well as the graphical display, in contour form, of the geoid grid. The program can draw the contour map of the geoid for any selected area with the option of annotating the interpolated random points on the map using different colors.

CHAPTER 5

THE UNIFIED GEOID FOR CANADA AND PART OF THE U.S.

Using the PC-based software package developed in this research, a unified geoid together with its error estimates has been computed for all of Canada and part of the U.S. All the computations were performed on a PC 486/50i computer with an expanded RAM of 20 MB and 330 MB of hard disk.

Section 5.1 describes the data sets used in this computation. Section 5.2 describes the results of geoid computation from a test run using data on a small subgrid both by the 1D spherical FFT and by direct summation to show the equivalence of the 1D spherical FFT algorithm to the direct evaluation of the discrete Stokes integral. Section 5.3 gives a brief description of the files containing the computed results and lists the simple statistics of the computed geoid files. In section 5.4, the computational efficiency of the 1D spherical FFT method is briefly discussed as compared to the direct summation in computing large scale continental geoids.

5.1 Data Sets Used

The data files used in the computation were all prepared and sent to us by the Geodetic Survey Division of Canada. They are the same sets of data as those used in computing the GSD91 geoid model (Veronneau and Mainville, 1992). The data sets include the following data files: a 5'x5' mean gravity anomaly grid corrected for the atmospheric effect and terrain correction, a reference gravity anomaly data grid and a reference geoidal undulation grid computed from the OSU91A geopotential model complete to degree and order 360. The grid size is 660x1320 (871200 grid points) covering all of Canada and part of the U.S., ranging from 35°N to 90°N in latitude and 210°E to 320°E in longitude. The average spacing of the surface gravity anomaly measurements used for gridding was about 10 km on land and 1 km over the oceans in Canada (Mainville and Veronneau, 1989). The gravity anomaly data are stored in three direct access binary files which also contain the standard deviations of the mean gravity anomalies and other information related to the gridding. To make the computation convenient, the three data files were combined into two data grids covering the whole area which contain the mean gravity anomalies and the corresponding standard deviations, respectively. In addition, a 1km x 1km digital terrain model for the Canadian Rockies was available. The GPS/levelling data in six GPS networks in Canada and two GPS networks in the U.S., which were used for comparison with the gravimetric geoid, were provided by the Geodetic Survey Division of Canada and the National Geodetic Survey of the U.S., respectively.

5.2 Results of Test Computation Using the 1D Spherical FFT Program

To show the equivalence of the 1D spherical FFT algorithm to the direct evaluation of the discrete Stokes integral and the correctness of the developed software, a test computation was carried out using data on a 50x50 subgrid located in the area of British Columbia (50°02'30"N to 54°07'30"N in latitude, 230°02'30"E to 234°07'30"E in longitude) both by the 1D spherical FFT algorithm and by the direct summation of the discrete Stokes integral. Table 5.1 lists the statistics of the residual part of the geoidal undulations computed by the two methods and table 5.2 contains the statistics of the differences of the geoidal undulations obtained by the 1D spherical FFT method with respect to the values obtained by direct summation, which are considered as the true values.

Table 5.1 Statistics of the Residual Part of the Geoid Undulations from the Test Computation Using Both the Direct Summation and the 1D Spherical FFT Method

Method Used	Min.	Max.	Mean	RMS	σ
	(m)				
Summation	-0,894	0.900	0.111	0.238	0.211
1D-FFT	-0.894	0.900	0.111	0.238	0.211

Table 5.2 Statistics of the Differences of Geoidal Undulations Between the 1D Spherical FFT Method and the Direct Summation

Differences	Min.	Max.	Mean	RMS	σ
	(m)				
1D-FFT Minus Summation	-1.8E-7	1.2E-7	3.1E-10	2.1E-8	2.1E-8

As shown in the above two tables, the 1D spherical FFT algorithm gives exactly the same results as those by direct evaluation of the discrete Stokes integral. The differences are of the order of about $2\text{x}10^{-7}$ m which are caused by the limitation of the computer word length and are completely negligible for our application.

5.3 Geoid Files Produced

The following files have been produced in this research: the geoid file UC93_1D.BIN (or simply called UC93) and the corresponding standard deviation file STD_CAN.BIN by 1D spherical FFT; the geoid file UC92_2DP.BIN (or simply called UC92) by 2D Planar FFT, and the geoid file UC92_2DS.BIN by 2D spherical FFT. The first geoid file covers the area of all of Canada and part of the U.S. with a grid size of 660 x 1320. The remaining two geoid files only cover the area of Canada which ranges from 41°N to 72°N in latitude and 218°E to 314°E in longitude with the grid size being 372 x 1152. The geoid file computed by 1D spherical FFT is the final product to be used by various users.

All the above files are direct access binary files with each record containing a real*4 number. The data are stored from north to south and from west to east for each latitude (the same way as the input data files). The results can also be stored as integer*2 binary files to save storage space as required.

In addition to the above geoid files, a file containing the indirect effects of up to second order of Helmert's condensation reduction for the mountainous area of British Columbia, called IND_BC.BIN, was produced using the digital terrain model. The grid size is 800 x 720 and the spacing is 32″ x 50″ , covering the area from 49°N to 56°N in latitude and 114°W to 124°W in longitude. The inclusion of the indirect effects does not show considerable improvement in the agreement between the gravimetric geoid and the GPS/levelling geoid because the GPS stations are located mostly in the valleys. But the indirect effects were still added to the geoid file UC93_1D.BIN since for the points on top of the mountains the indirect effects are not negligible (the value may reach as much as half a metre as shown in table 5.5).

Table 5.3 gives a brief list of the files described above.

Table 5.3 Files Produced in this Research

File Name	TYPE	Area	Grid Size
UC92_2DP	Geoid	All Canada	373 x1152
UC92_2DS	Geoid	All Canada	373 x 1152
UC93_1D	Geoid	All Canada and Part of U.S.	660 x 1320
STD_CAN	Internal Error Estimates	All Canada and Part of U.S.	660 x 1320
IND_CAN	Indirect Effects	B.C.	800 x 720

Table 5.4 lists the statistics of the three geoid files. Table 5.5 contains the statistics of the geoid error standard deviations contributed by the anomaly data noise. In table 5.6 are the statistics of the indirect effects.

Table 5.4 Statistics of the Three Geoid Files Computed

FILE NAME	MIN	MAX	MEAN	RMS	σ
	(m)				
UC93_1D	-48.534	50.991	-4.990	23.237	22.694
UC92_2DP	-48.893	44.152	-15.333	25.125	19.904
UC92_2DS	-48.813	43.878	-15.250	25.023	19.838

Table 5.5 Statistics of the Geoid Noise Contributed by the Gravity Anomaly Data Noise

FILE NAME	MIN	MAX	MEAN	RMS	σ
	(m)				
STD_CAN	0.017	0.278	0.095	0.117	0.068

Table 5.6 Statistics of the Indirect Effect of Helmert's Condensation Reduction

FILE NAME	MIN	MAX	MEAN	RMS	σ
	(m)				
IND_BC	-0.523	0.000	-0.101	0.126	0.075

As shown in table 5.5, the undulation error contributed by the gravity anomaly data noise is, on the average, about 10 cm with a maximum value of 28 cm. The variation is about 7 cm (1σ). The larger undulation errors are mainly due to lack of gravity data coverage in some area. It should be mentioned that the undulation errors were obtained through error propagation using the given a priori variances of the anomaly data noise while the real accuracy of the computed geoid should be evaluated by comparing it to the independent external information such as the GPS/levelling-derived geoid. As will be shown later in chapter 6, the error estimates from the error propagation compare well with actual error estimates from the external comparison.

Figure 5.1 and Figure 5.2 shows the UC93 geoid in all of Canada and its internal error estimates contributed from the gravity anomaly data noise, respectively. To demonstrate the long wavelength and short wavelength features of the geoid, Figure 5.3 and Figure 5.4 show the geoid derived from OSU91A model and the residual part of the geoid in the area of Western Canada.

5.4 The Computation Efficiency of the 1D Spherical FFT Method

The major advantage of the FFT-based techniques for evaluating the discrete convolutions in physical geodesy is its remarkable speed. The 1D spherical FFT technique for geoid computation is not only rigorously equivalent to the direct summation of the discrete Stokes integral but also far more efficient in terms of computation time. To show this, the CPU time required for calculating the geoidal undulations at all the grid points on a 660x1320 grid (Canada and part of U.S.) and a 373x1152 grid (only Canada) both by the direct summation method and the 1D Spherical FFT method were recorded using a Lahey system subroutine. All the computations were made on a 486/50i PC computer. Table 5.6 and table 5.7 list the CPU time spent for evaluating the two geoid grids. Note that the CPU time for the direct summation method is obtained by multiplying the CPU time required for computing one point with the total number of grid points.

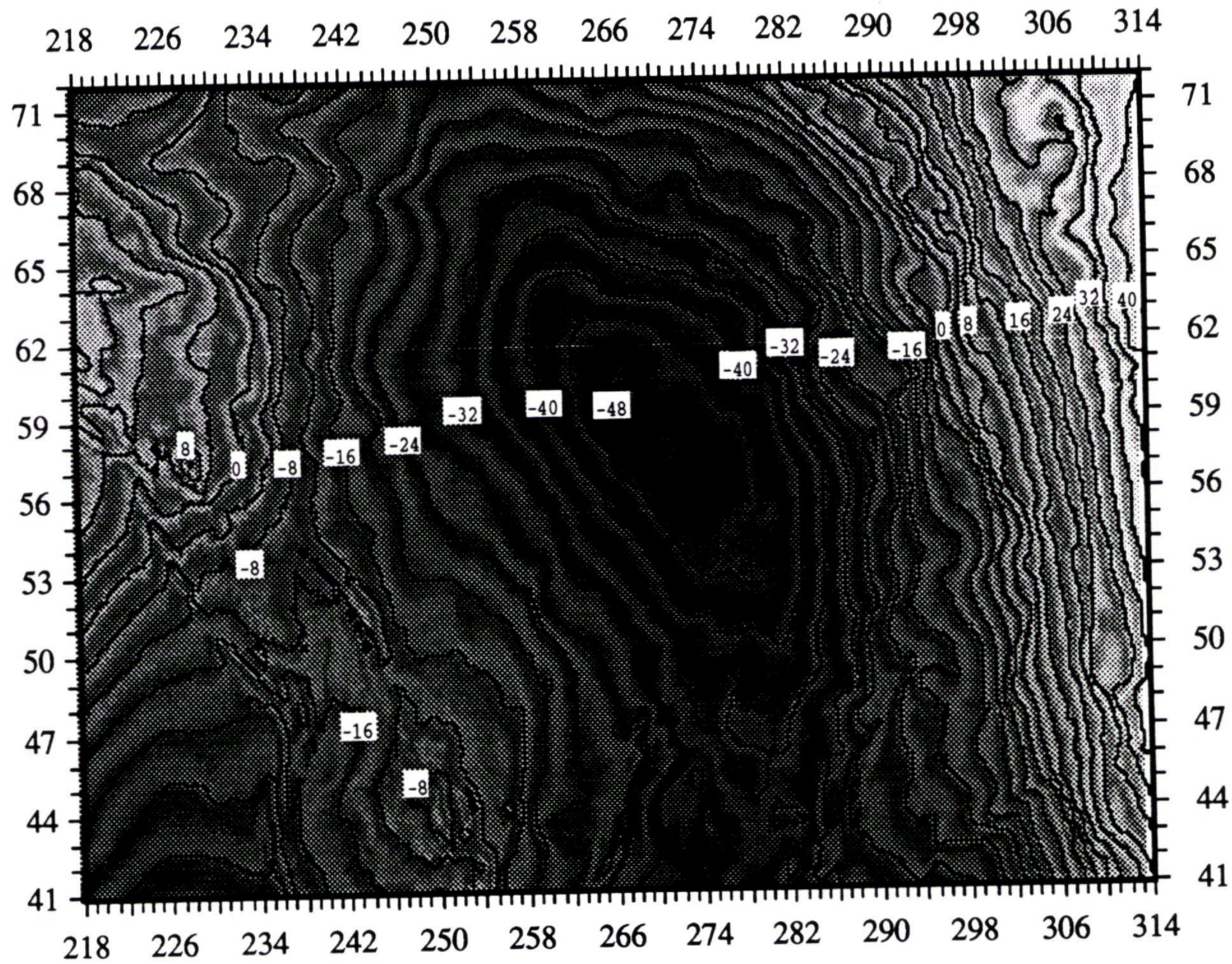

Figure 5.1 UC93 Geoid for All of Canada

(Contour Interval: 4 m)

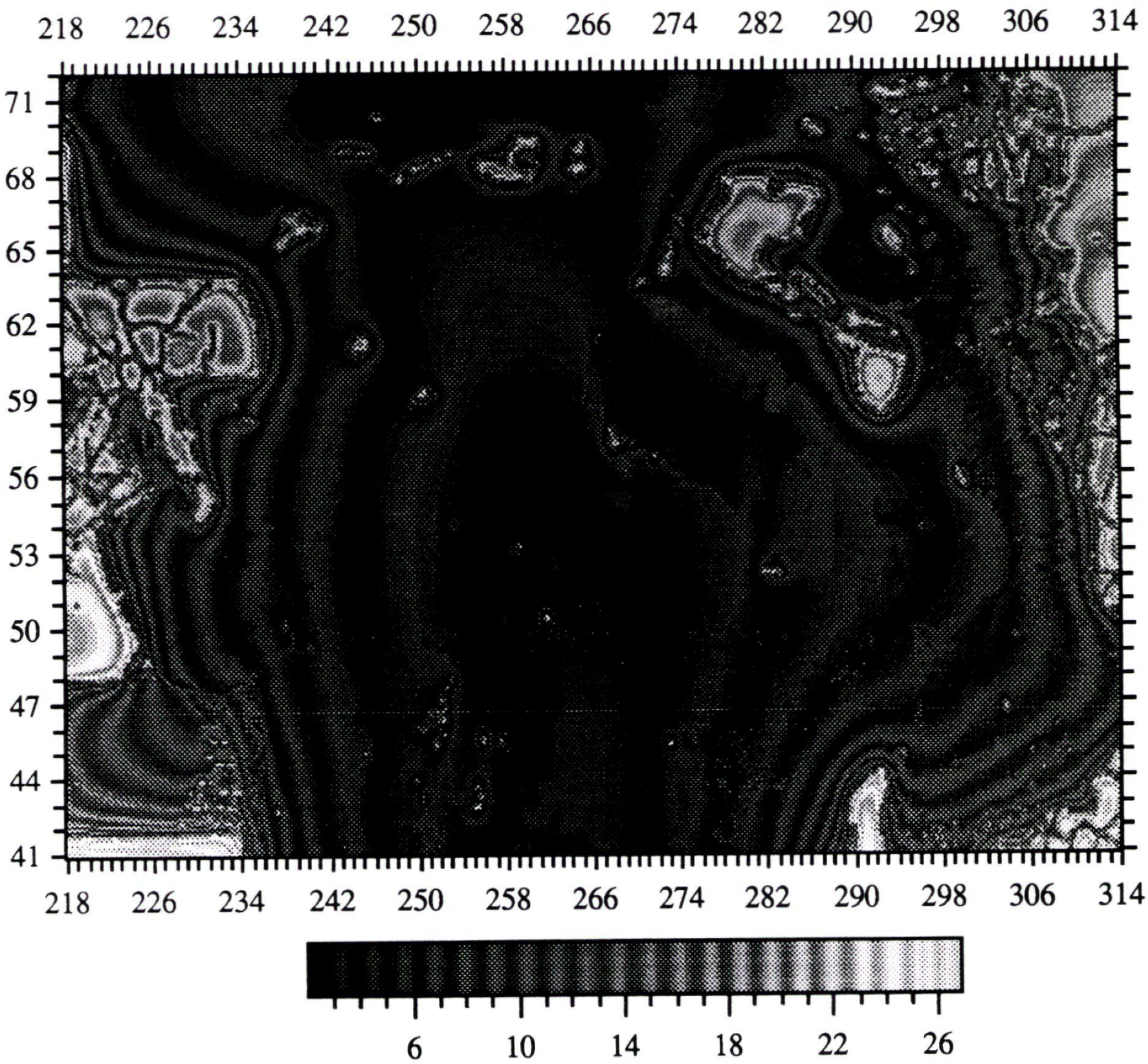

Figure 5.2 Internal Geoidal Undulation Errors Contributed by the Gravity Anomaly Data Noise [cm]

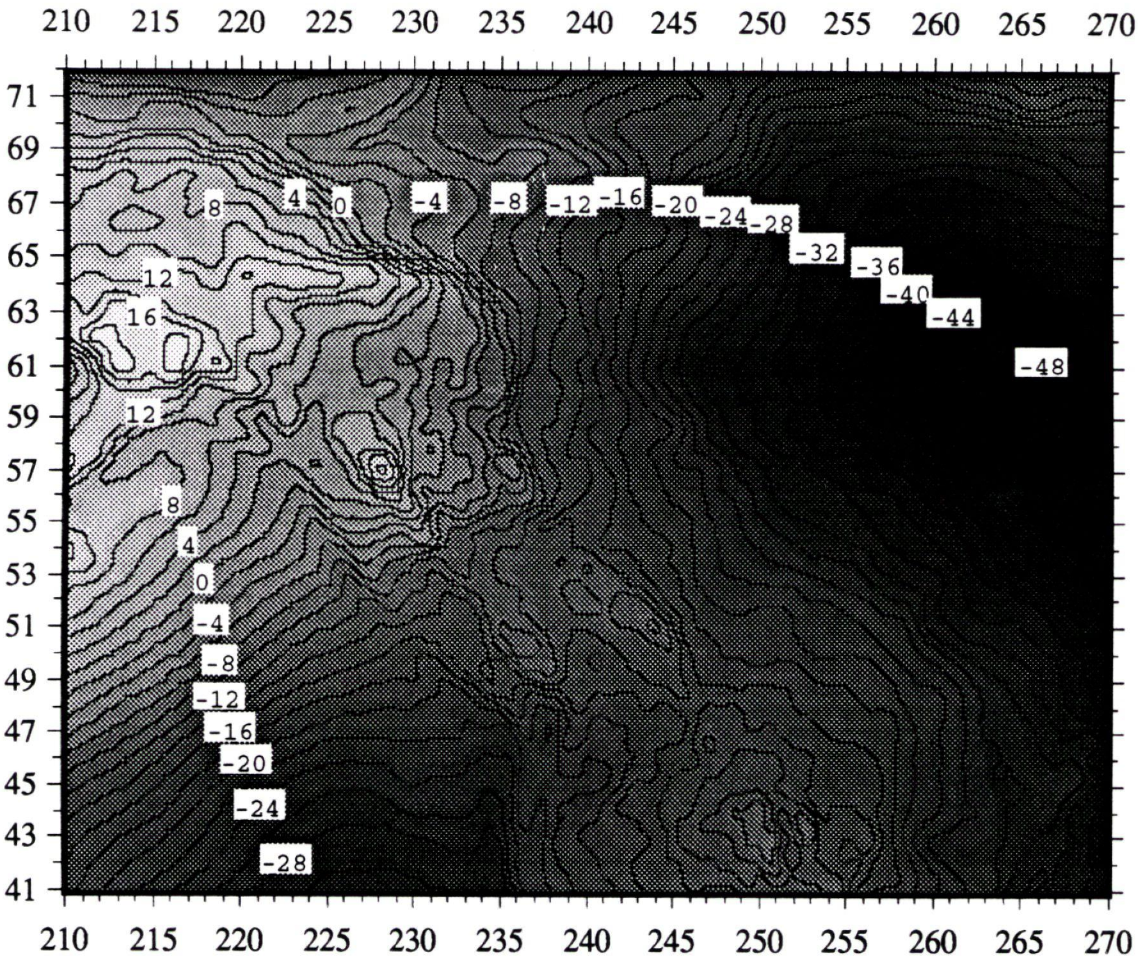

Figure 5.3 Geopotential model contribution, N_{GM} (long wavelengths).
(contour interval: 2 m)

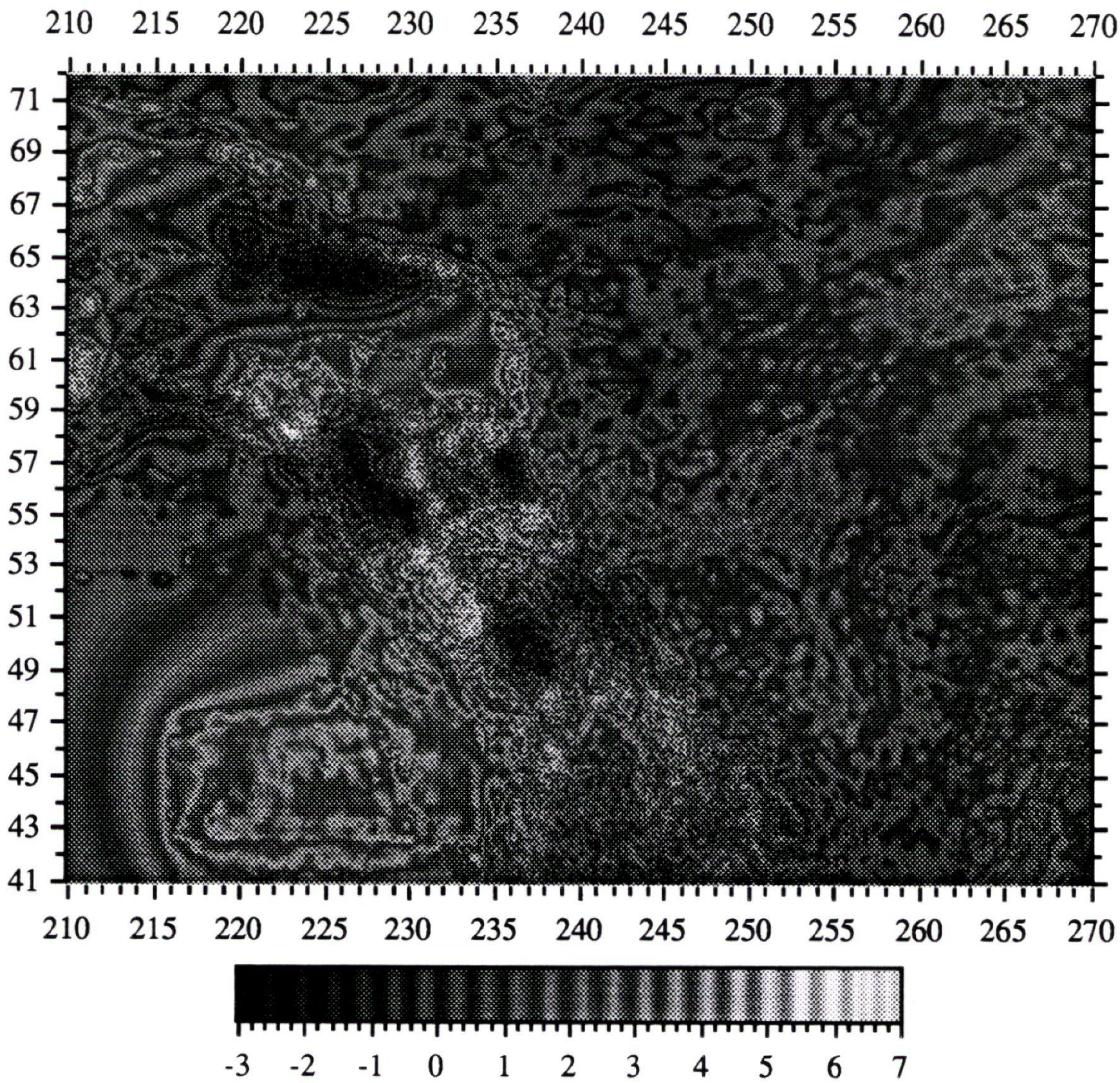

Figure 5.4 Contribution of gravity anomalies and heights, $N_{\Delta g}+N_{ind}$ (medium and short wavelengths).

Table 5.7 CPU Time for Evaluating the 660x1320 Geoid Grid

Method	CPU Time in Hours
1D Spherical FFT	70.58
Direct Summation	15112.9

Table 5.8 CPU Time for Evaluating the 373x1152 Geoid Grid

Method	CPU Time in Hours
1D Spherical FFT	16.39
Direct Summation	3712.86

As shown in these tables, the CPU time required by the direct summation method is over 200 times that by the FFT method. For the 660x1320 grid the CPU time required by the direct summation method is about 629.7 days (almost two years) while it needs only about 2.9 days with the FFT method. These numbers definitely show how much time can be saved using the FFT-based methods when dealing with the problem of calculating large-scale continental geoid such as the current Canadian geoid. This result also shows that it is now practically possible to evaluate large-scale local or regional geoid accurately at high speed on low-cost microcomputers. Note that the above time does not include the time required for read/write data and results, which is the same for each of the above two methods.

CHAPTER 6

RESULTS OF COMPARISONS BETWEEN THE GRAVIMETRIC AND THE GPS/LEVELLING-DERIVED GEOIDAL UNDULATIONS

To evaluate the accuracy of the computed geoid, data from eight local GPS networks in Canada and U.S together with the levelling data were used to derive the geoidal undulations for comparison with the gravimetric geoidal heights. Statistics of the GPS networks are shown in table 6.1. To show the distribution of GPS stations in the area of Canada, contour maps of the geoid annotated with GPS points for Western Canada and the Ontario/Quebec area were plotted using the PLOTCTR program, as shown in Figures 6.1 and 6.2, respectively

The geoidal height from GPS/levelling data is computed simply by

$$N = h - H, \tag{80}$$

where h is the ellipsoidal height derived from GPS and H is the orthometric height from levelling. To get the real picture of the agreement of the gravimetric geoid with respect to the GPS/levelling data, the systematic datum difference between the gravimetric geoid and the GPS/levelling data and the possible long wavelength errors of the geoid were removed by the following 4-parameter transformation equation (Heiskanen and Moritz, 1967):

$$N' = N + b_0 + b_1 \cos\varphi \cos\lambda + b_2 \cos\varphi \sin\lambda + b_3 \sin\varphi \quad , \tag{81}$$

where b_0 is the shift parameter between the vertical datum implied by the GPS/Levelling data and the gravimetric datum, and b_1, b_2, b_3 are the three translation parameters in x,y,z axes between the coordinate system implied by the GPS data and that by the gravimetric data. The program STAT allows for selection of different combinations of one to four parameters in (81) to get the best fit.

Table 6.1 Statistics of Eight GPS Networks in Canada and the U.S.

Area	Geographical Range		No. of Stations	Time of obs.
	Latitude(DEG)	Longitude(DEG)		
British Columbia	49N - 61N	114W - 130W	280	1989
Northern Alberta	56N - 60N	111W - 121W	51	1990
Central Alberta	54N - 56N	110W - 120W	52	1990
Southern Alberta	49N - 54N	110W - 116W	107	1991
Great Slave Lake	60N - 63N	111W - 118W	93	1987
Ontario/Quebec	42N - 46N	70W - 83W	228	1988
Washington State	46N - 49N	117W - 124W	62	1988
Oregon State	42N - 46N	117W - 124W	15	1988

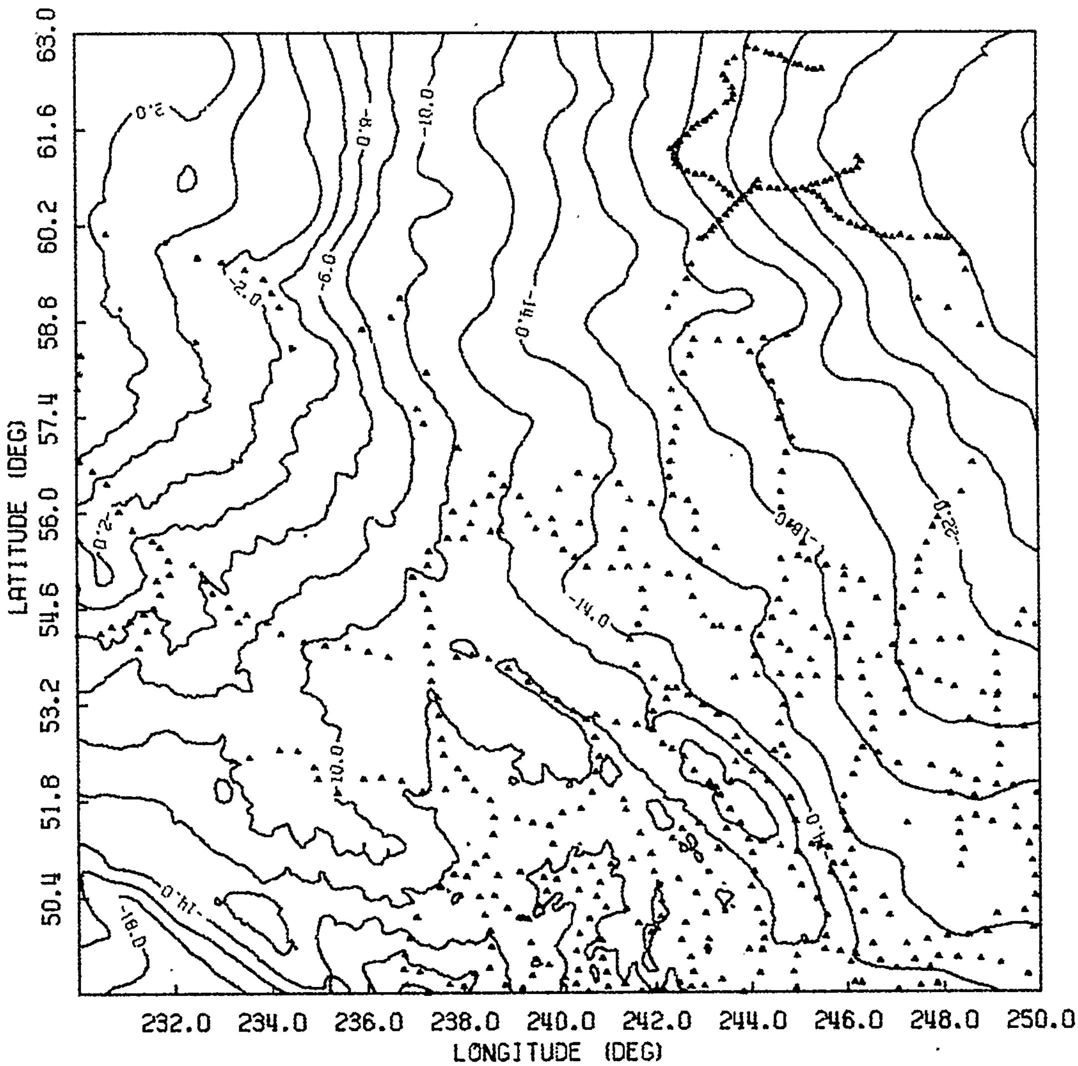

Figure 6.1 Contour Map of Geoidal Undulations Annotated with GPS Stations for Western Canada

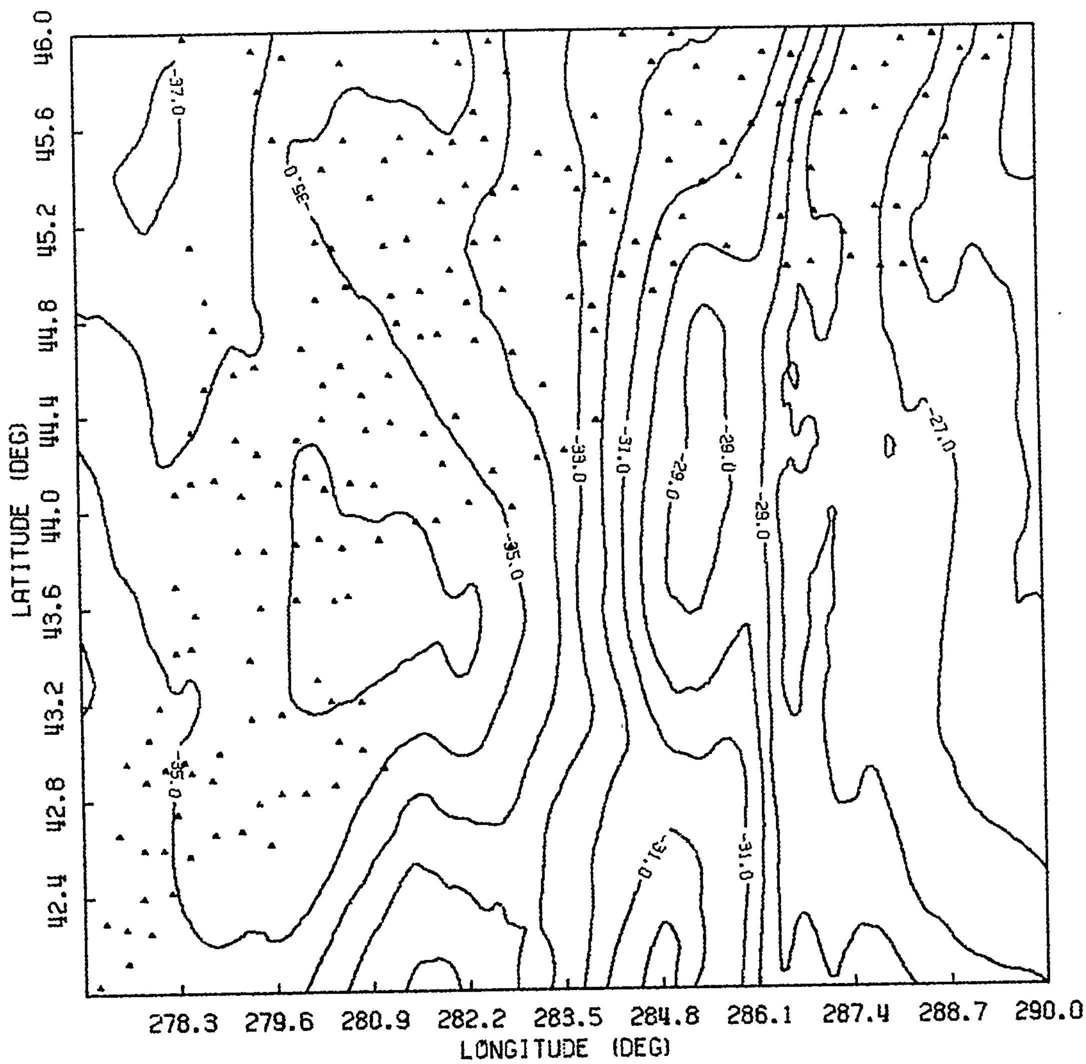

Figure 6.2 Contour Map of Geoidal Undulations Annotated with GPS Stations for Ontario/Quebec

Six geoid models were used in the comparison. These models are: OSU91A, UNB90 by the University of New Brunswick, GEOID90 by the National Geodetic Survey of the U.S., GSD91 by the Geodetic Survey Division of Canada, UC92 (UC92_2DP or planar 2D FFT) and UC93 (spherical 1D FFT) by the author.

Both the absolute comparison and the relative comparison were made between the gravimetric geoid and the GPS/levelling-derived geoid. Subsection 6.1 describes the results of the absolute comparisons. The results of relative comparisons are in subsection 6.2. Subsection 6.3 gives a comparison of different geoid models in terms of approximation error and agreement with GPS/levelling data.

6.1 The Absolute Accuracy of the Gravimetric Geoid with Respect to the GPS/Levelling-Derived Geoidal Undulations

The statistics of the absolute differences between the two types of geoidal heights for the eight local GPS networks are summarized in tables 6.2 to 6.9. The numbers in parentheses refer to the results before removing the datum differences.

Statistics of the Differences between the Gravimetric and GPS/Levelling Geoidal Heights

Table 6.2a Area: British Columbia No. of Points: 280

GEOID MODEL	MIN	MAX	MEAN	RMS	σ
	(m)				
OSU91A	-4.74(-7.43)	2.78(0.07)	0.00(-2.77)	0.98(2.94)	0.98(0.98)
UNB90	-1.51(-2.87)	2.19(2.44)	0.00(-0.13)	0.72(1.26)	0.72(1.25)
GSD91	-1.58(-5.52)	1.17(-2.29)	0.00(-3.05)	0.30(3.09)	0.30(0.52)
UC92	-1.28(-5.81)	0.89(-2.69)	0.00(-3.48)	0.27(3.52)	0.27(0.52)
UC93	-1.29(-6.39)	0.70(-3.35)	0.00(-4.08)	0.24(4.11)	0.24(0.53)

Table 6.2b Area: British Columbia No. of Points: 203

GEOID MODEL	MIN	MAX	MEAN	RMS	σ
	(m)				
OSU91A	-2.46	2.40	0.00	0.77	0.77
UNB90	-1.47	2.19	0.00	0.71	0.71
GSD91	-0.41	0.31	0.00	0.15	0.15
UC92	-0.32	0.29	0.00	0.12	0.12
UC93	-0.19	0.18	0.00	0.10	0.10

Table 6.3 Area: Northern Alberta No. of Points: 51

GEOID MODEL	MIN	MAX	MEAN	RMS	σ
	(m)				
OSU91A	-0.37(-0.47)	0.46(0.74)	0.00(0.26)	0.17(0.39)	0.17(0.29)
UNB90	-0.18(-0.11)	0.12(0.86)	0.00(0.27)	0.07(0.34)	0.07(0.21)
GSD91	-0.23(-0.29)	0.13(0.12)	0.00(-0.84)	0.06(0.08)	0.06(0.08)
UC92	-0.20(-0.39)	0.14(0.03)	0.00(-0.23)	0.05(0.24)	0.05(0.08)
UC93	-0.19(-0.99)	0.13(-0.57)	0.00(-0.84)	0.06(0.85)	0.06(0.08)

Table 6.4 Area: Central Alberta No. of Points: 52

GEOID MODEL	MIN	MAX	MEAN	RMS	σ
	(m)				
OSU91A	-0.22(-0.27)	0.21(0.23)	0.00(-0.02)	0.10(0.12)	0.10(0.12)
UNB90	-0.19(-0.53)	0.33(0.59)	0.00(0.10)	0.10(0.28)	0.10(0.27)
GSD91	-0.16(-0.87)	0.15(-0.45)	0.00(-0.58)	0.05(0.59)	0.05(0.07)
UC92	-0.11(-0.99)	0.16(-0.57)	0.00(-0.76)	0.05(0.76)	0.05(0.07)
UC93	-0.12(-1.54)	0.17(-1.14)	0.00(-1.33)	0.05(1.33)	0.05(0.07)

Table 6.5a Area: Southern Alberta No. of Points: 106

GEOID MODEL	MIN	MAX	MEAN	RMS	σ
	(m)				
OSU91A	-0.65(0.18)	0.46(1.36)	0.00(0.65)	0.16(0.69)	0.16(0.22)
UNB90	-0.42(0.10)	1.22(3.57)	0.00(1.24)	0.22(1.41)	0.22(0.68)
GSD91	-0.09(-0.25)	0.25(0.86)	0.00(0.27)	0.05(0.34)	0.05(0.21)
UC92	-0.10(-0.38)	0.12(0.41)	0.00(0.09)	0.04(0.20)	0.04(0.17)
UC93	-0.10(-0.92)	0.13(-0.11)	0.00(-0.46)	0.04(0.48)	0.04(0.16)

Table 6.5b Area: Southern Alberta No. of Points: 100

(With six points deleted)

GEOID MODEL	MIN	MAX	MEAN	RMS	σ
	(m)				
OSU91A	-0.33	0.44	0.00	0.14	0.14
UNB90	-0.34	0.55	0.00	0.18	0.18
GSD91	-0.08	0.12	0.00	0.04	0.04
UC92	-0.10	0.09	0.00	0.03	0.03
UC93	-0.08	0.09	0.00	0.03	0.03

Table 6.6 Area: Great Slave Lake No. of points: 93

GEOID MODEL	MIN	MAX	MEAN	RMS	σ
	(m)				
OSU91A	-0.16(-0.60)	0.35(0.73)	0.00(-0.13)	0.10(0.35)	0.10(0.32)
UNB90	-0.19(-0.39)	0.23(0.52)	0.00(-0.07)	0.07(0.20)	0.07(0.18)
GSD91	-0.16(-0.37)	0.16(0.44)	0.00(-0.08)	0.05(0.19)	0.05(0.17)
UC92	-0.16(-0.58)	0.20(0.31)	0.00(-0.27)	0.05(0.34)	0.05(0.20)
UC93	-0.16(-1.21)	0.21(-0.27)	0.00(-0.90)	0.06(0.92)	0.06(0.21)

Table 6.7a Area: Ontario/Quebec No. of points: 228

GEOID MODEL	MIN	MAX	MEAN	RMS	σ
	(m)				
OSU91A	-1.03(1.13)	1.49(1.30)	0.00(0.06)	0.27(0.34)	0.27(0.34)
UNB90	-1.21(-0.85)	0.83(1.23)	0.00(0.29)	0.23(0.39)	0.23(0.26)
GSD91	-1.28(-1.42)	1.35(1.22)	0.00(-0.03)	0.23(0.26)	0.23(0.26)
UC92	-1.18(-0.91)	1.39(1.63)	0.00(0.25)	0.23(0.35)	0.23(0.24)
UC93	-1.19(-1.19)	1.36(1.30)	0.00(0.02)	0.23(0.25)	0.23(0.25)

Table 6.7b Area: Ontario/Quebec No. of points: 197

(With 31 points deleted)

GEOID MODEL	MIN	MAX	MEAN	RMS	σ
	(m)				
OSU91A	-0.59(0.51)	0.54(0.72)	0.00(0.01)	0.19(0.26)	0.19(0.25)
UNB90	-0.31(-0.25)	0.36(0.70)	0.00(0.0.28)	0.12(0.32)	0.12(0.17)
GSD91	-0.26(-0.34)	0.24(0.37)	0.00(-0.05)	0.10(0.15)	0.10(0.14)
UC92	-0.24(-0.13)	0.26(0.53)	0.00(0.22)	0.10(0.25)	0.10(0.12)
UC93	-0.22(-0.33)	0.25(0.38)	0.00(0.00)	0.10(0.13)	0.10(0.13)

Table 6.8 Area: Washington State No. of Points: 61

GEOID MODEL	MIN	MAX	MEAN	RMS	σ
	(m)				
OSU91A	-0.96(-1.63)	1.22(0.53)	0.00(-0.77)	0.42(0.91)	0.42(0.48)
UNB90	-0.48(-0.83)	0.57(1.78)	0.00(0.45)	0.24(0.75)	0.24(0.61)
GEOID90	-0.24(-1.44)	0.37(0.30)	0.00(-0.81)	0.10(0.84)	0.10(0.23)
GSD91	-0.35(-2.02)	0.21(-1.23)	0.00(-1.90)	0.09(1.91)	0.10(0.14)
UC92	-0.26(-2.36)	0.22(-1.50)	0.00(-0.46)	0.09(0.48)	0.09(0.17)
UC93	-0.22(-2.98)	0.15(-2.16)	0.00(-2.49)	0.08(2.50)	0.08(0.18)

Table 6.9 Area: Oregon State No.of Points: 15

GEOID MODEL	MIN	MAX	MEAN	RMS	σ
	(m)				
OSU91A	-0.34(-1.78)	0.44(-0.67)	0.00(-1.13)	0.22(1.19)	0.22(0.37)
UNB90	-0.23(-1.12)	0.40(0.28)	0.00(-0.45)	0.15(0.59)	0.15(0.38)
GEOID90	-0.13(-1.61)	0.18(-0.99)	0.00(-1.31)	0.10(1.33)	0.10(0.21)
GSD91	-0.14(-1.92)	0.19(-1.12)	0.00(-1.62)	0.10(1.63)	0.10(0.20)
UC92	-0.14(-2.21)	0.17(-1.69)	0.00(-1.99)	0.09(2.00)	0.09(0.14)
UC93	-0.14(-2.48)	0.19(-2.10)	0.00(-2.55)	0.09(2.56)	0.09(0.20)

As shown in these tables, the geoid model computed by the 1D spherical FFT method agrees with the GPS/levelling data to better than 10 cm (RMS) in all GPS networks except the one in British Columbia and the one in Ontario/Quebec. In BC, this is due to the rough terrain and poor gravity data coverage in part of the province (Northwest corner). In Ontario/Quebec, the GPS results on a small portion of the stations are very poor and there are also some gravity gaps in part of the area. The best agreement is achieved in Southern Alberta where the RMS error is 4 cm for the whole set of 106 points (Table 6.5a) and reduces to only 3 cm after 6 noisy points with differences larger than 10 cm are eliminated (Table 6.5b). In the area of Northern and Central Alberta as well as in the Great Slave Lake region, the agreement is at the level of 5 cm to 6 cm (Table 6.3, 6.4, 6.6.). For the two GPS networks located in the state of Washington and Oregon in the U.S., the agreement is 8 cm and 9cm, respectively (Tables 6.8 and 6.9). In British Columbia, the statistics made on all 280 stations of the network show an RMS error of 24 cm (Table 6.2a).

But a detailed analysis shows that this large rms error mainly comes from the contribution of a small portion of the points. Table 6.10 gives the percentage of points falling into different ranges of errors for the UC93 (1D FFT) geoid model.

Table 6.10 Distribution of Points in Different Error Ranges in British Columbia for UC93 Geoid Model

Error Limit (m)	No. of Points	Cumulative Percentage	RMS Error (m)
0.10	118	42.0%	0.06
0.20	203	72.5%	0.10
0.30	249	88.9%	0.14
0.40	256	91.4%	0.15
0.50	262	93.6%	0.16
0.70	271	96.8%	0.19
1.30	280	100%	0.24

As shown in the table, over 70% of the points in the network have a 10 cm RMS agreement with respect to the GPS/levelling data. The agreement is better than 15cm RMS for 90% of the points. Only 8.6% of the points (24 stations) have differences larger than 40cm which increases the RMS error from 15cm to 24cm. Some of these noisy points are in the area where there is no surface gravity coverage (Northwest corner of BC). More careful investigations are required as to the real causes of the large differences at these points.

In the Ontario/Quebec area, the statistics made on all stations of the network (228 points) shows an RMS error of 23 cm (table 6.7a). But a detailed analysis shows that this large RMS error is mainly from the contribution of a small number of stations in the network. Table 6.11 gives the percentage of points falling into different ranges of errors for the UC93 (1D FFT) geoid model.

Table 6.11 The Distribution of Points in Different Error Ranges in Ontario/Quebec for UC93 Geoid Model

Error Limits (m)	No. of Points	Cumulative Percentage	RMS Error (m)
0.10	134	58.8%	0.06
0.20	188	82.4%	0.09
0.25	197	86.4%	0.10
0.30	205	89.9%	0.11
0.40	209	91.7%	0.12
0.50	217	95.2%	0.15
1.40	228	100%	0.23

As shown in the table, over 86% of the points in the network has a 10 cm RMS agreement with respect to GPS/levelling data. The agreement is better than 12 cm RMS for about 92% of the points. Only 8.3% of the points (19 stations) have differences larger than 40cm which increases the RMS error from 12 cm to 23 cm. 4.8% of the stations (11 stations) have differences ranging from 0.5 m to 1.4 m, bringing the RMS error from 15 cm to 23 cm. These 11 points are believed to have gross errors coming from GPS/levelling data. More careful examinations are required to diagnose the real causes of the large differences at these points.

It should be mentioned that the above accuracy of the gravimetric geoid with respect to the GPS/levelling datum is obtained after removing the datum difference through a least-squares fit using eq. (81) where all the data points in each network are used. To further verify the reliability of the accuracy estimates thus obtained, the datum difference is removed only using the data in a portion of the points in a network each time. Table 6.12 shows the statistics of the absolute comparison after performing datum transformation using different number of data points in the GPS network in British Columbia.

Table 6.12 Statistics of the Differences between the Gravimetric Geoid and the GPS/levelling Geoid after Removing the Datum Difference by LS Fit Using Different Numbers of Data Points

No. of Fitted Points	MIN	MAX	MEAN	RMS	σ
	(m)				
none	-6.39	-3.35	-4.08	4.11	0.53
4	-1.30	0.78	0.06	0.26	0.25
15	-1.36	0.72	0.00	0.26	0.26
60	-1.32	0.82	0.02	0.25	0.25
140	-1.20	0.81	0.03	0.24	0.24
200	-1.18	0.78	0.01	0.24	0.24
280	-1.29	0.70	0.00	0.24	0.24

As shown in the table, the statistics of the accuracy of the gravimetric geoid with respect to the GPS/levelling datum after fitting with different number of data points are basically the same. This result indicates that there exists a significant datum difference between the gravimetric geoid and the GPS/levelling geoid. A LS fit using only a few points (larger or equal to 4 points) will usually be enough to remove the datum differences. This result is of practical importance when one uses GPS heights and gravimetric geoidal undulations to obtain orthometric heights instead of levelling since only a few benchmarks occupied by GPS receivers are required to obtain the necessary transformation parameters.

To investigate whether there is a correlation between the above external errors of the gravimetric geoid and the internal errors obtained by propagating the measurement noise of the gravity anomaly data onto the geoid, statistics of the internal errors were computed for each area where the GPS networks are located using the results in file STD_CAN.BIN. Table 13 lists the statistics for the eight GPS networks used in the comparison.

Table 6.13 Statistics of the Internal Geoidal Undulation Errors Contributed from the Measurement Noises of the Anomaly Data (Unit: metre)

Area	Max.	Min	Mean	σ	RMS
British Columbia	0.203	0.036	0.059	0.029	0.066
Northern Alberta	0.056	0.033	0.042	0.005	0.042
Central Alberta	0.047	0.032	0.038	0.004	0.038
Southern Alberta	0.041	0.031	0.035	0.002	0.035
Great Slave Lake	0.168	0.036	0.048	0.021	0.053
Ontario	0.234	0.035	0.057	0.024	0.062
Washington	0.068	0.042	0.051	0.006	0.051
Oregon	0.163	0.044	0.057	0.009	0.058

Comparing the results in the above table with those in tables 6.2 to table 6.8, we see a strong correlation between the external errors and the internal errors. As can be seen from table 13, the highest precision occurs in the area of Alberta where the effect of the gravity anomaly noise on the geoid is about 3.5 to 4 cm and very uniform (notice the small variations), showing a remarkable consistency with the results of the external comparison. In accordance with the results of the external comparison, the internal precision in the area of

British Columbia and the Ontario/Quebec area is the worst (at the level of about 6cm) and show relatively larger variations than other areas. The maximum standard deviation reaches over 20 cm, which may be caused by the lack of data coverage in the neighborhood of these points and is one reason for the large discrepancies of the gravimetric geoidal undulations with respect to GPS/levelling results.

To examine the possible correlation between the topography and the accuracy of the geoid, simple statistics of the topographic heights were also made for each area. Table 6.14 lists the results.

Table 6.14 Statistics of the Topographic Heights for the Eight Areas Where GPS Networks are Located (Unit: Metre)

Area	Max.	Min	Mean	σ	RMS
British Columbia	2719	-2925	99	673	1123
Northern Alberta	1067	176	510	195	546
Central Alberta	1846	435	726	187	749
Southern Alberta	2587	557	989	389	1063
Great Slave Lake	808	91	223	239	85
Ontario	1244	-128	259	166	308
Washington	2704	-194	682	480	833
Oregon	2392	-50	1064	518	1184

As shown in the table, it seems that there is little correlation between the topographic variations (roughness) and the accuracy of the geoid. This is not surprising, and just shows that the topography and its indirect effect have been properly modelled.

To study the influence of indirect effects upon the accuracy of the geoid, comparisons were made using the data in the area bounded by 49°N - 56°N latitude and 114°W - 124°W longitude in British Columbia. The available GPS stations in the area are 203. Table 6.15 gives the results of the comparison with and without adding the indirect effects to the geoid. The geoid file is UC93_1D.BIN. Three cases were considered: case 1: no indirect effects added; case 2: indirect effect of the first term added; case 3: indirect effect of both the first and second term added.

Table 6.15 Statistics from Comparison Between the gravimetric and the GPS/levelling Geoid Undulations With and Without the Indirect Effects

Area: B.C.(LAT. 49°N-56°N, LON. 114°W-124°W) No. of GPS Points: 203

CASE	MIN	MAX	MEAN	RMS	σ
	(m)				
CASE 1	-0.58(-4.54)	0.80(-3.35)	0.00(-3.82)	0.18(3.83)	0.18(0.24)
CASE 2	-0.59(-4.51)	0.79(-3.28)	0.00(-3.77)	0.18(3.78)	0.18(0.25)
CASE 3	-0.60(-4.54)	0.79(-3.28)	0.00(-3.77)	0.18(3.78)	0.18(0.25)

As shown in the table, the addition of indirect effects only affects the mean difference slightly but have no influence on the RMS error. Case 2 and case 3 have the same results, indicating that the effect of the second-term is negligible. The GPS stations used in above comparison are in the valleys, however, larger effects are expected for stations at mountain peaks. Thus, it is recommended to properly take into account the indirect effects in such extreme cases.

To sum up the analyses in this section, we conclude that the absolute agreement of the newly computed geoid with respect to the GPS/levelling datum is at the level of 10 cm or better areas with good gravity coverage.

6.2 The Relative Accuracy of the Gravimetric Geoid With Respect to the GPS/Levelling-Derived Geoidal Undulations

To evaluate the relative accuracy of the gravimetric geoid with respect to the GPS/levelling data, relative differences were formed on all the baselines of different lengths in each network and plotted against distance both in units of one part per million (ppm) and metres as shown in figure 6.3 to figure 6.12. Note that the relative accuracy value at a certain distance is the average value of all the baselines of about the same length in each network, with an increment of about 20 km.

As seen in these figures, for the UC93 geoid model computed by the 1D spherical FFT, the relative agreement is, in most cases, about 1 to 4 ppm over short baselines of 20 to 100km, 0.5 to 1ppm for distances of 100 to 200km, and 0.1 to 0.5 ppm over distances of 200km to more than 1000km.

Best relative agreements are achieved for the three networks in the Province of Alberta, where the relative agreement is about 0.5 to 2ppm, 0.3 to 0.5ppm, 0.1 to 0.3 ppm for the above distances (fig. 6.5, fig. 6.6 and fig. 6.7).

In British Columbia, due to the roughness of topography and lack of gravity data in some parts of the area, the relative agreement is poorer than in other networks. Figure 6.3 shows the relative agreement computed from the data of all 280 points in the network where the RMS error of absolute agreement is 24 cm. It can be seen that the relative agreement is about 8.7 to 2 ppm for distances of 20 km to 100 km, 2 to 1ppm for distances of 100 to 240 km, 1 to 0.5 ppm for distances of 250 to 500 km, and 0.5 to 0.3 ppm for distances of 500 to 1700 km. However, for most of the stations in the network, the agreement is much better. Figure 6.4 shows the results of statistics on 203 points where the absolute differences are all below 20 cm corresponding to a RMS error of 10 cm. As shown in the figure, the relative agreement is about 4.1 to 1.3 ppm, 1.3 to 0.5 ppm, 0.5 to 0.2 ppm, 0.2 to 0.1 ppm or less for the above distance ranges.

In the Ontario/Quebec network, due to a few noisy GPS stations, the relative agreement based upon the data from all 228 stations where the absolute agreement is 0.23 m RMS is poor. As shown in figure 6.9, the relative agreement is about 5.7 to 2 ppm for distances of 20 km to 100 km, 2 to 1 ppm for distances of 100 to 200 km, 1 to 0.5 ppm for distances of 200 to 400 km, and 0.5 to 0.3 ppm for distances of 400 to 1000 km. Figure 6.10 shows the results of statistics from 197 stations where the absolute agreement is 10 cm RMS. As shown in this figure, the relative agreement is about 3 to 1 ppm, 1 to 0.7 ppm, 0.7 to 0.3 ppm, 0.3 to 0.1 ppm for the above distance ranges.

It is also noted that the relative agreement between the newly computed regional gravimetric geoid and the GPS/levelling-derived geoidal undulations is quite uniform in each network and no significant trend dependent on baseline length can be seen, as shown in figures 6.3b to 6.13b. In most cases, the relative error of the gravimetric geoid with respect to the GPS/levelling datum is smaller than 15 cm for baselines of tens of kilometres to over 1500 kilometres. In areas with good gravity data coverage and mild terrain, the error is smaller than 10 cm. In the area of Alberta Province, the relative error is only 5 to 6 cm (fig. 5b, 6b and 7b). However the relative error of the geoid implied by the global geopotential model OSU91A shows an increasing trend with baseline length (as clearly shown in fig. 4b and table 3.2). This might be due to the long wave-length error of the geopotential model. This result indicates that the combination of high-degree geopotential model and local gravity data can overcome the long wave length error of the geopotential model and result in geoid of uniformly high accuracy.

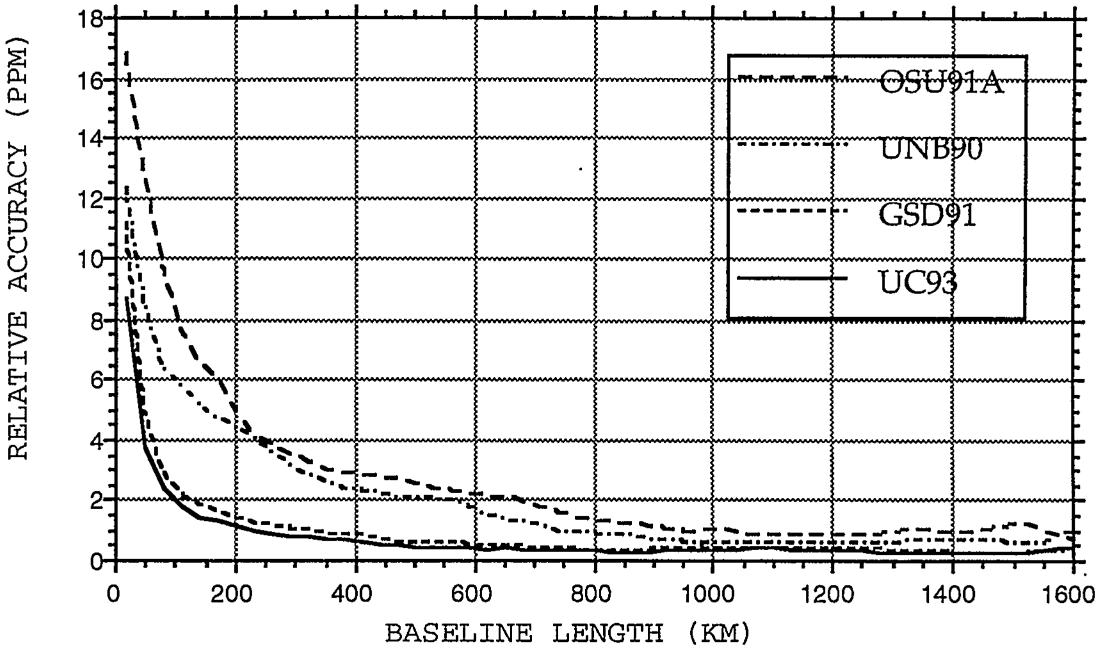

Figure 6.3a. Relative undulation Accuracy in British Columbia (280 Points), in ppm

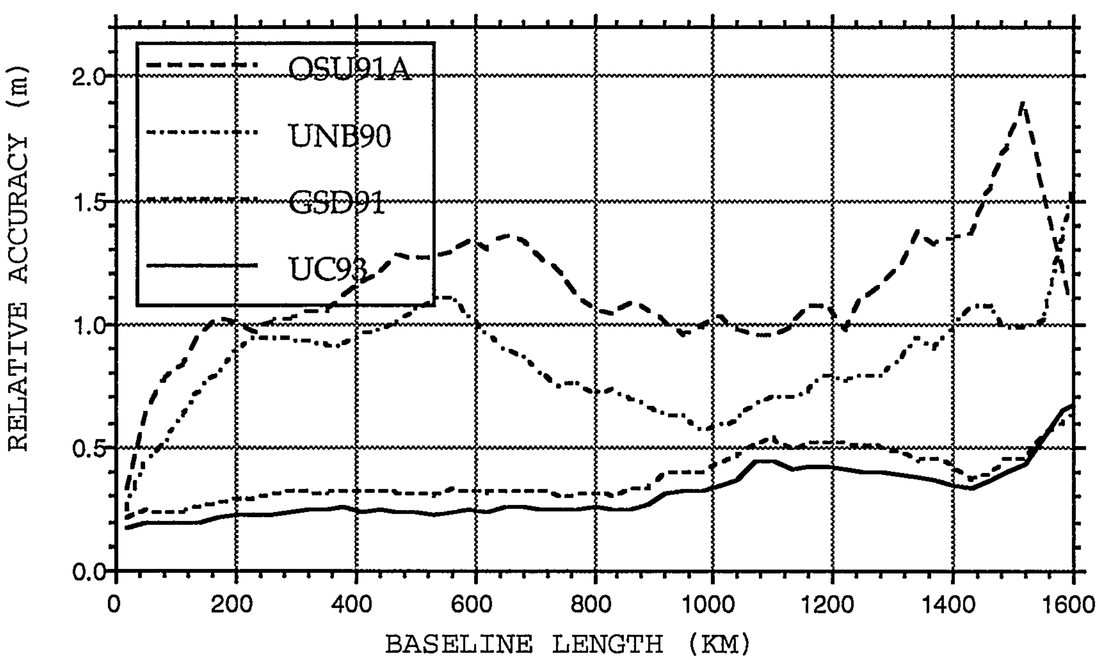

Figure 6.3b. Relative Undulation Accuracy in British Columbia(280 Points), in metre

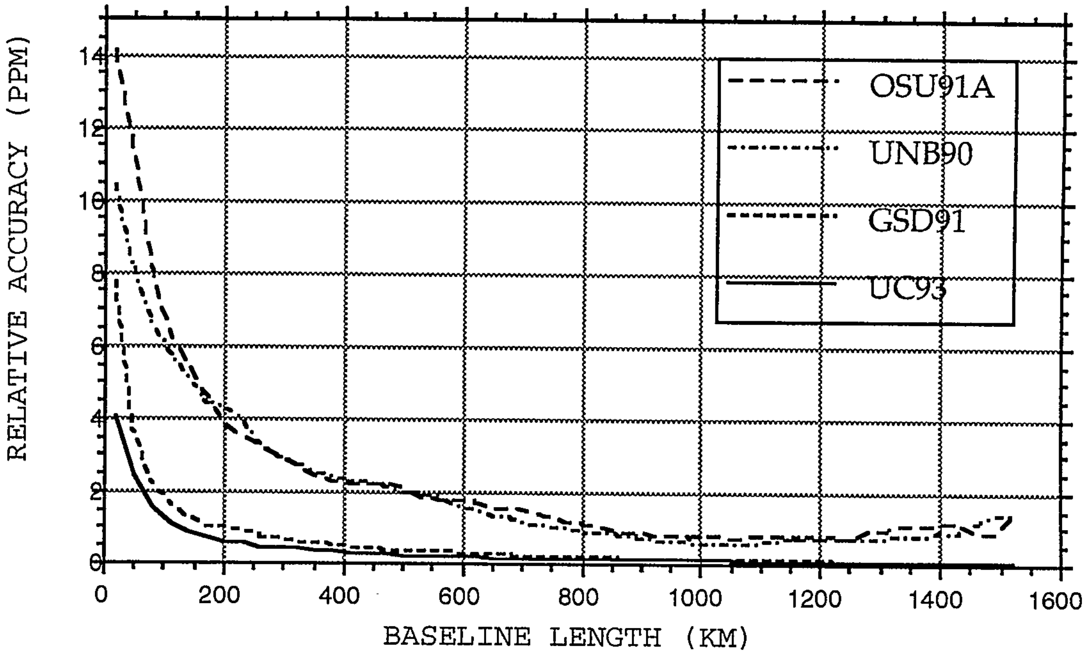

Figure 6.4a. Relative Undulation Accuracy in British Columbia (203 Points), in ppm

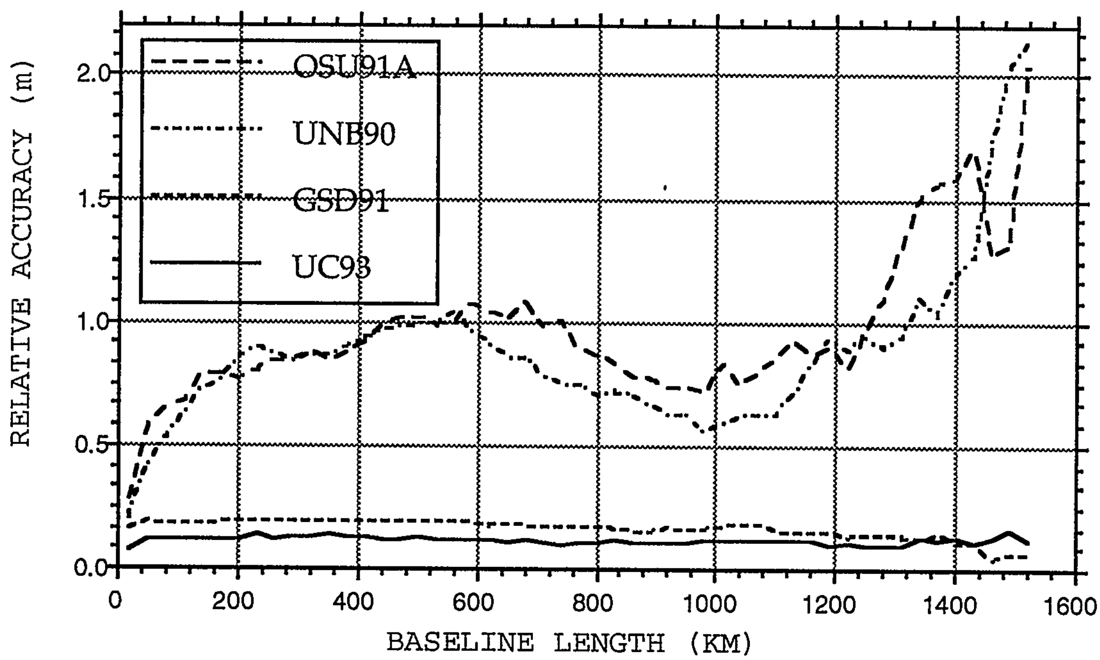

Figure 6.4b Relative Undulation Accuracy In British Columbia (203 Points), in metre

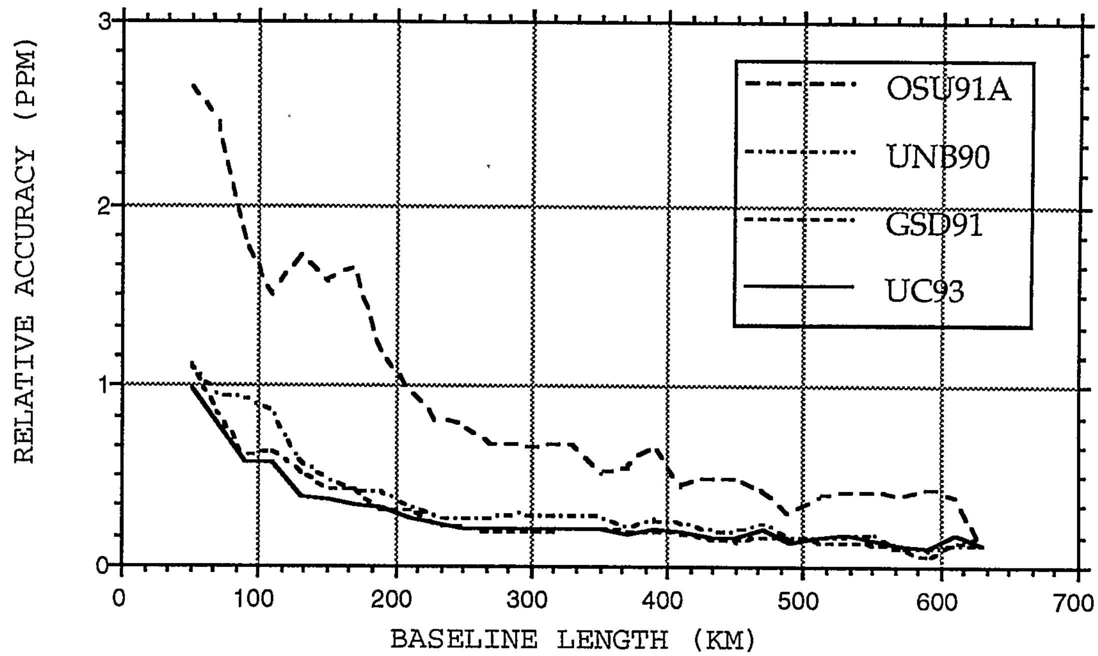

Figure 6.5a. Relative Undulation Accuracy in Northern Alberta, in ppm

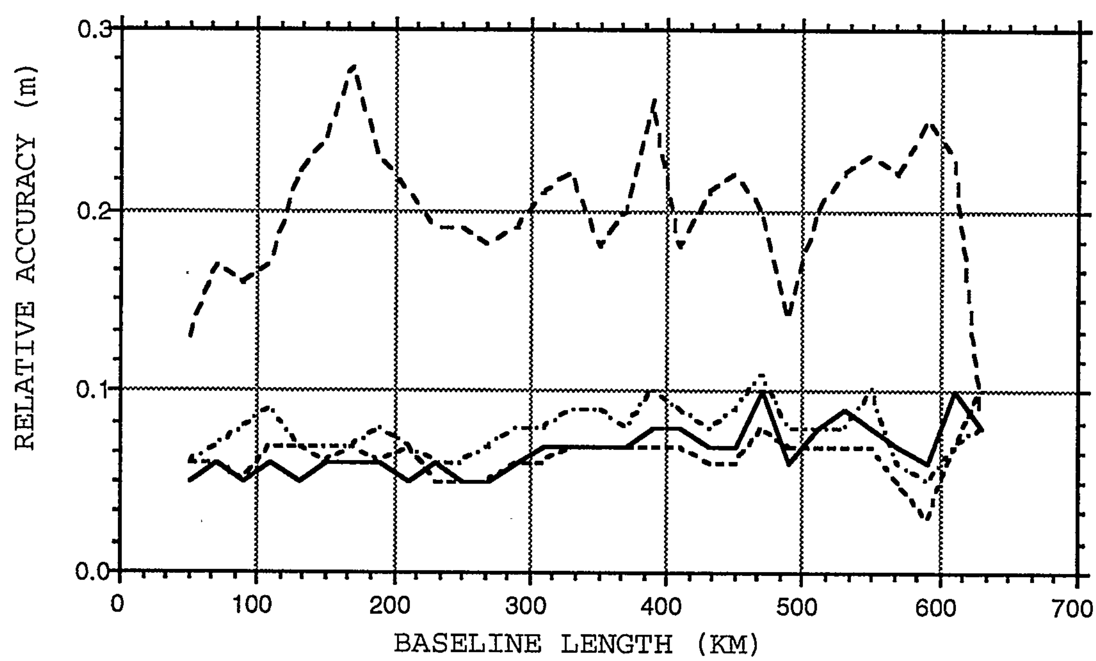

Figure 6.5b. Relative Undulation Accuracy in Northern Alberta, in metre

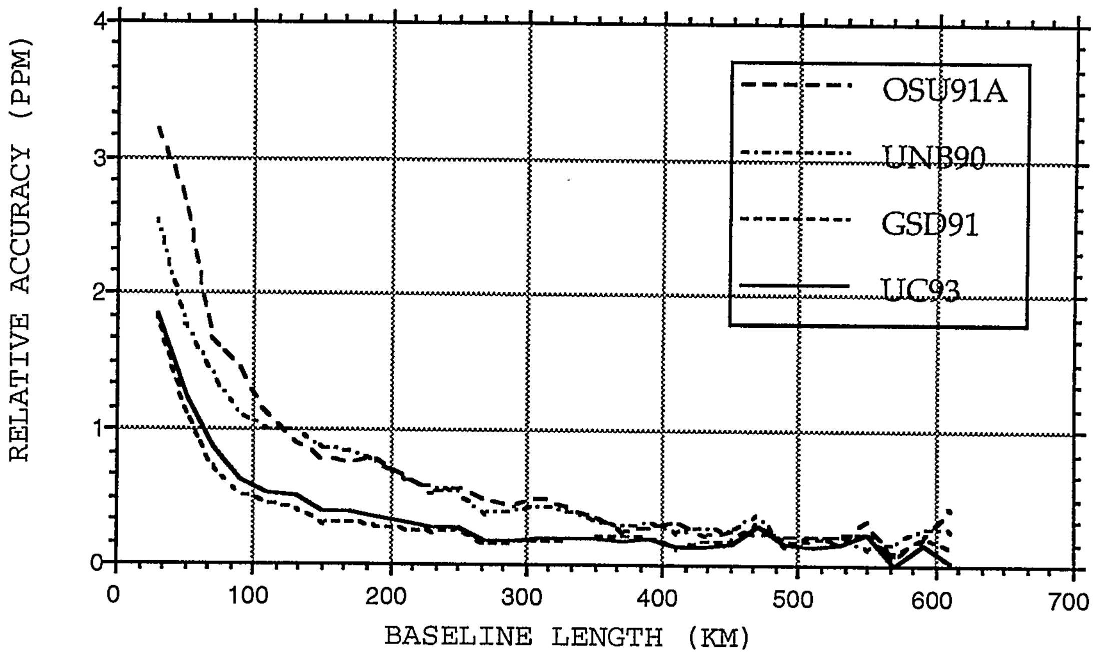

Figure 6.6a. Relative Undulation Accuracy in Central Alberta, in ppm

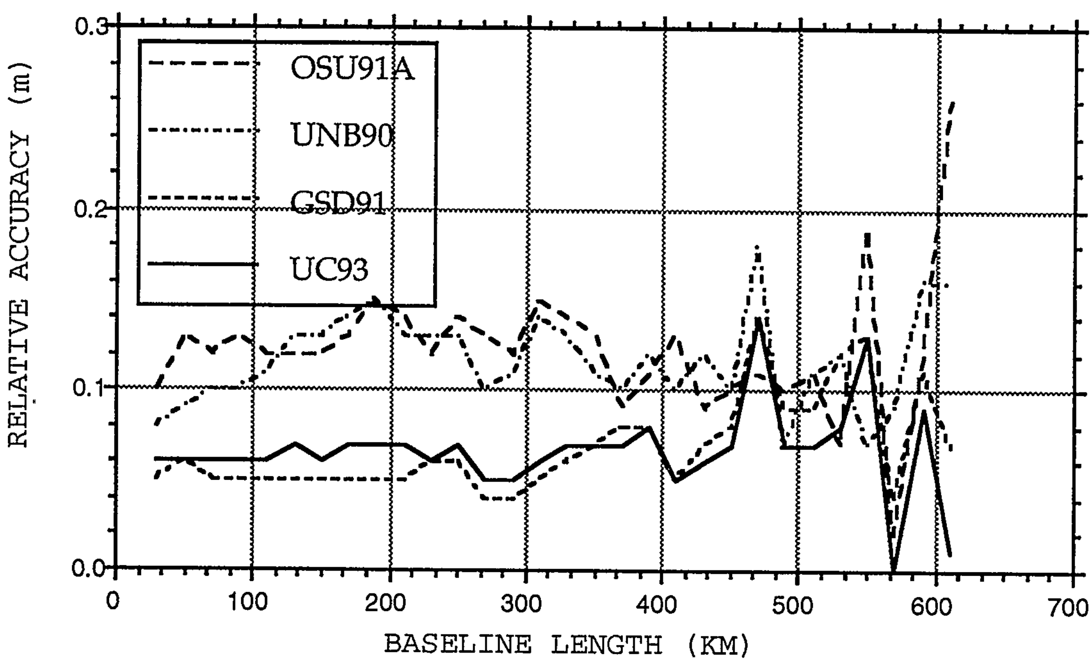

6.6b. Relative Undulation Accuracy in central Alberta, in metre

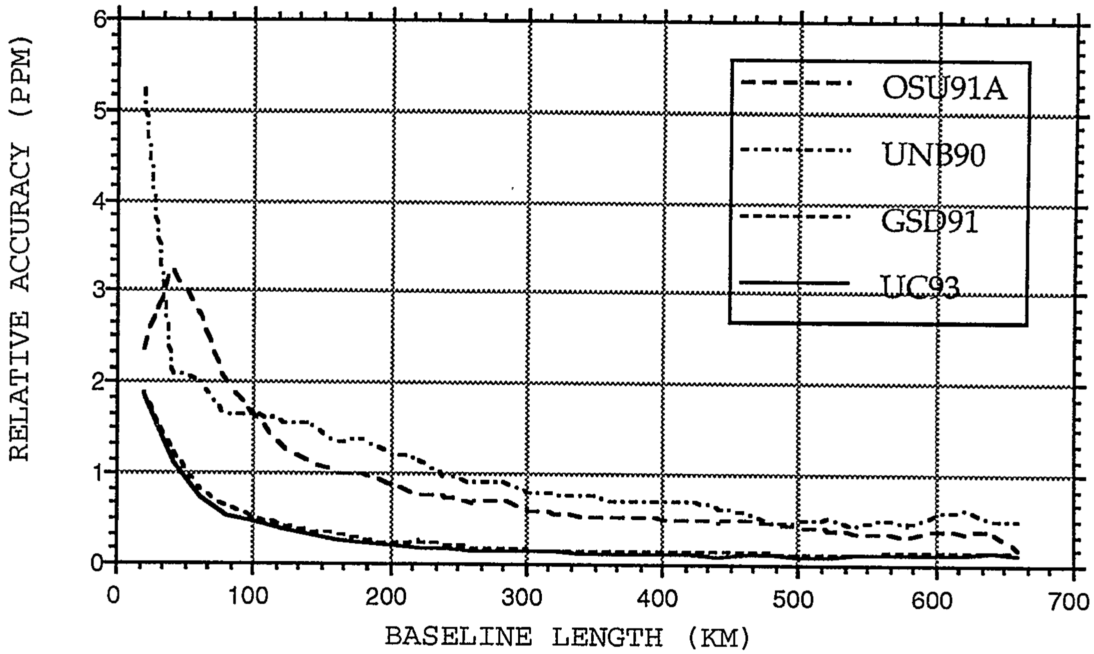

Figure 6.7a. Relative Undulation Accuracy in Southern Alberta, in ppm

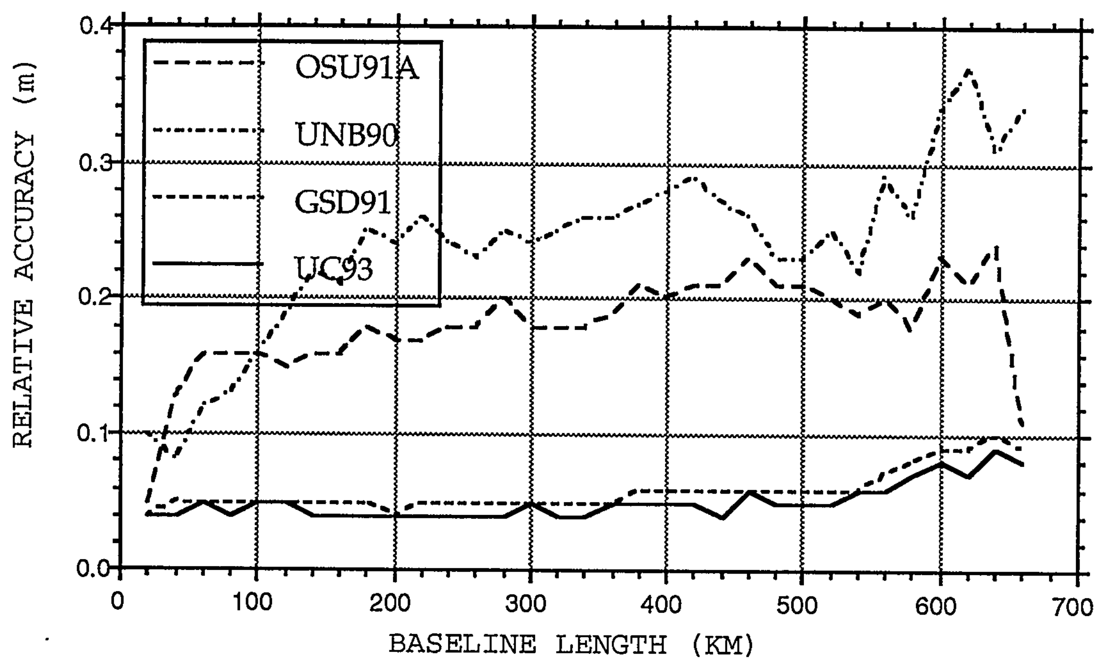

Figure 6.7b. Relative Undulation Accuracy in Southern Alberta, in metre

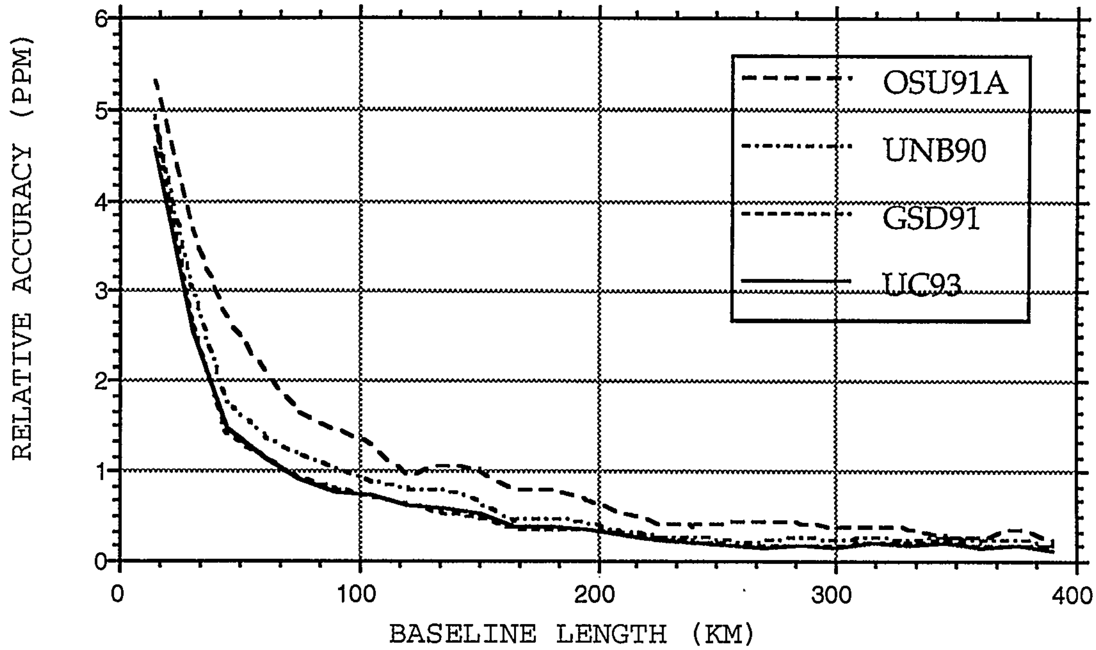

Figure 6.8a. Relative Undulation Accuracy in Great Slave Lake Area, in ppm

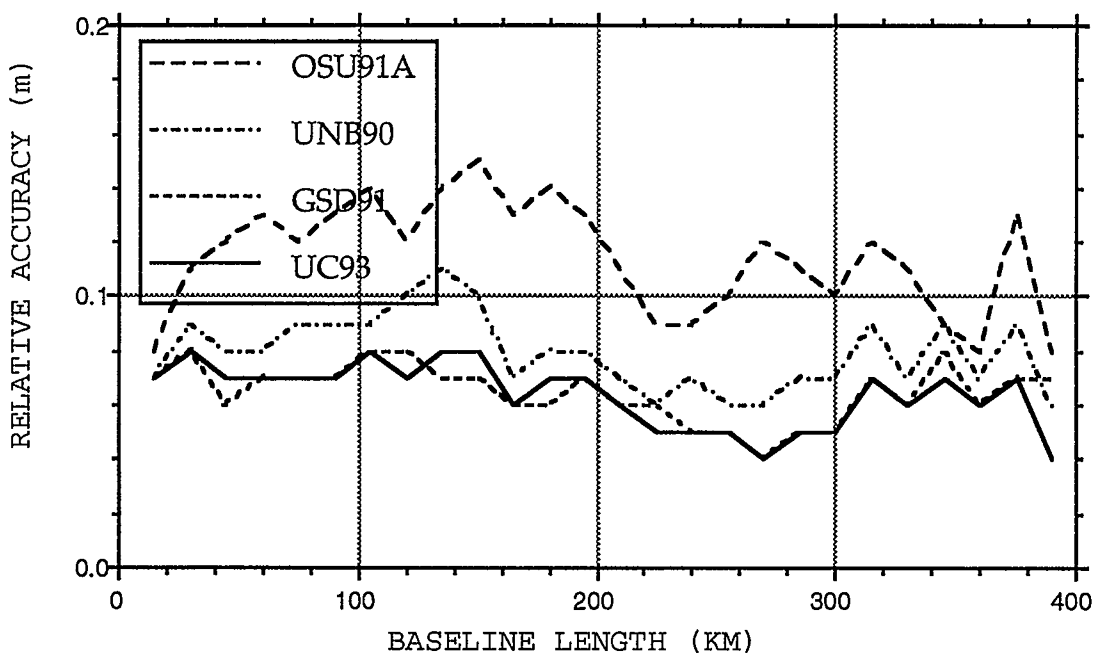

Figure 6.8b. Relative Undulation Accuracy in Great Slave Lake Area, in metre

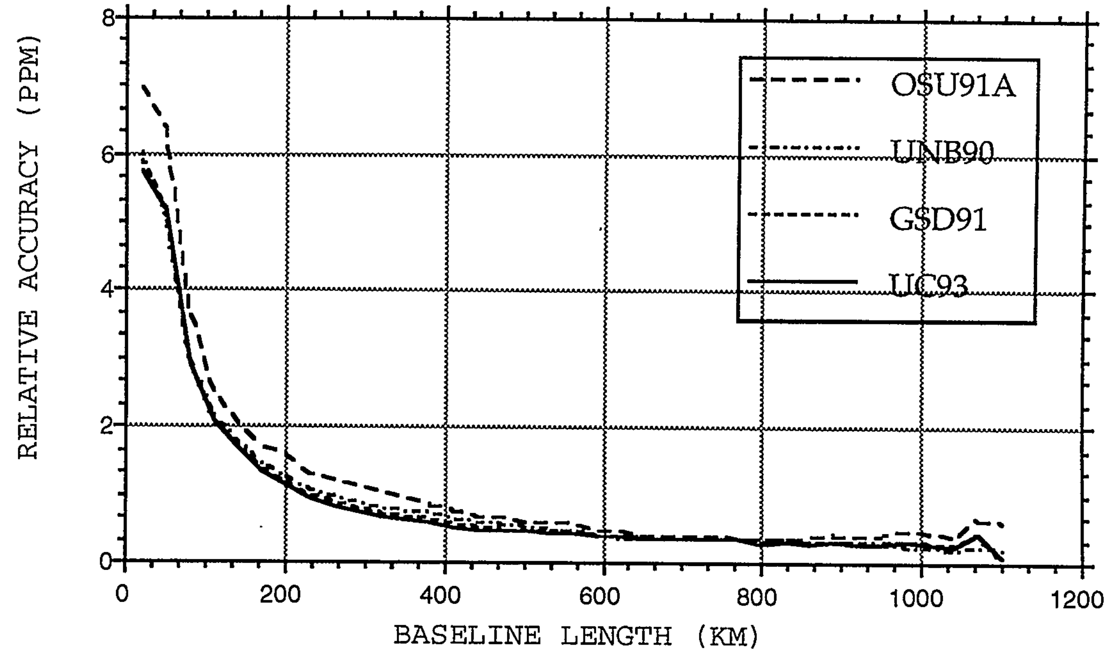

Figure 6.9a. Relative Undulation Accuracy in Ontario/Quebec (228 Points), in ppm

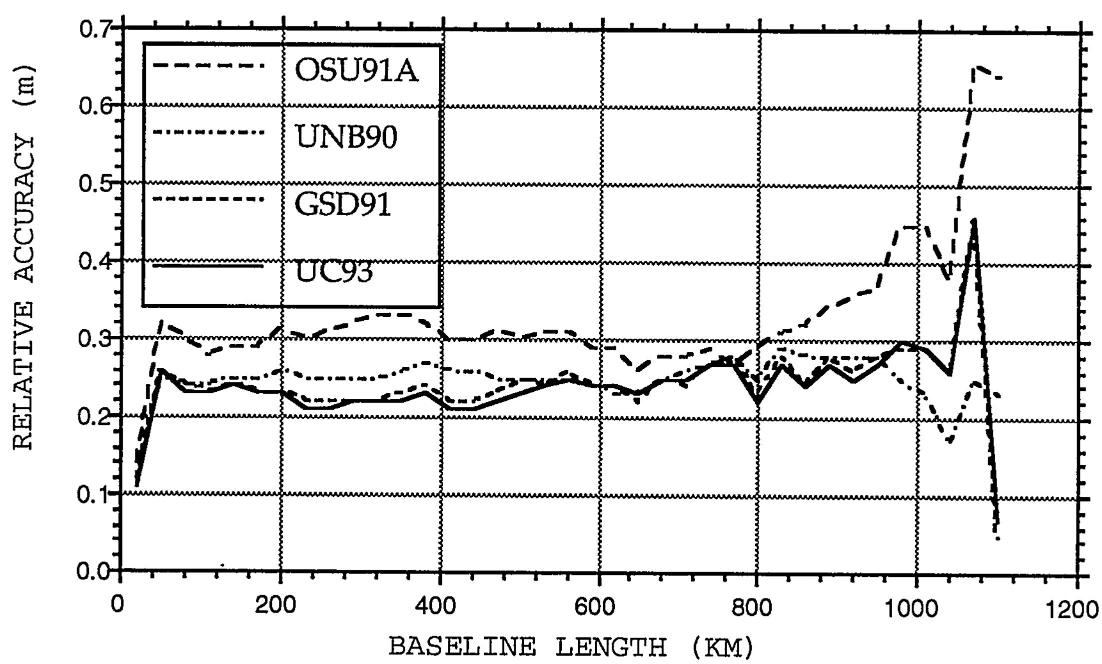

Figure 6.9b. Relative Undulation Accuracy in Ontario/Quebec (228 Points), in metre

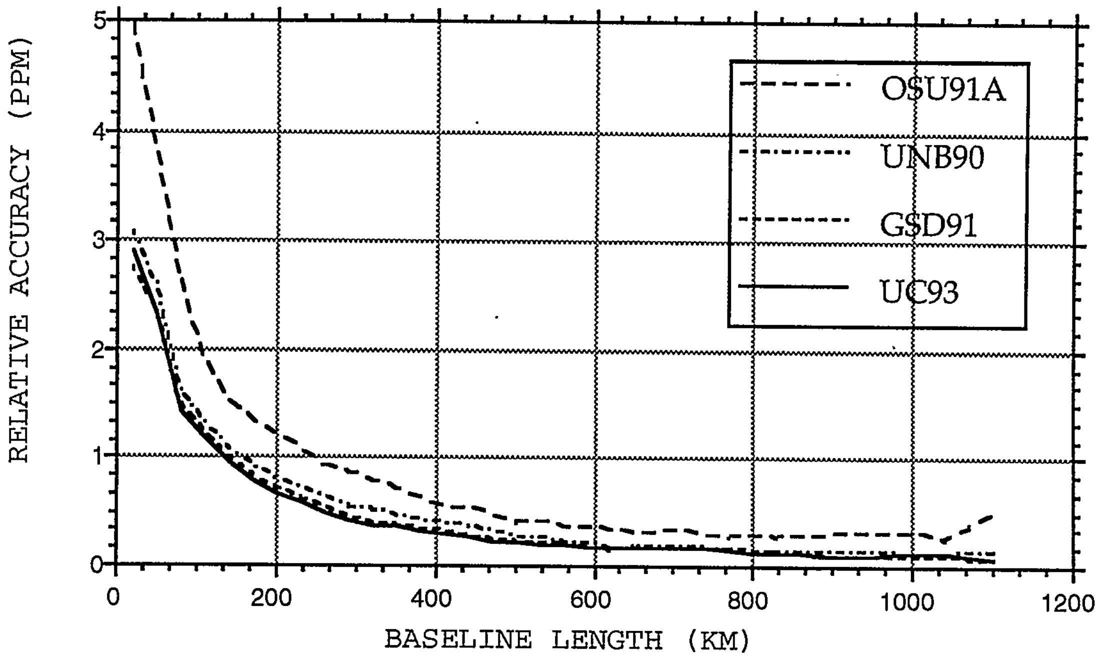

Figure 6.10a Relative Undulation Accuracy in Ontario/Quebec (203 Points), in ppm

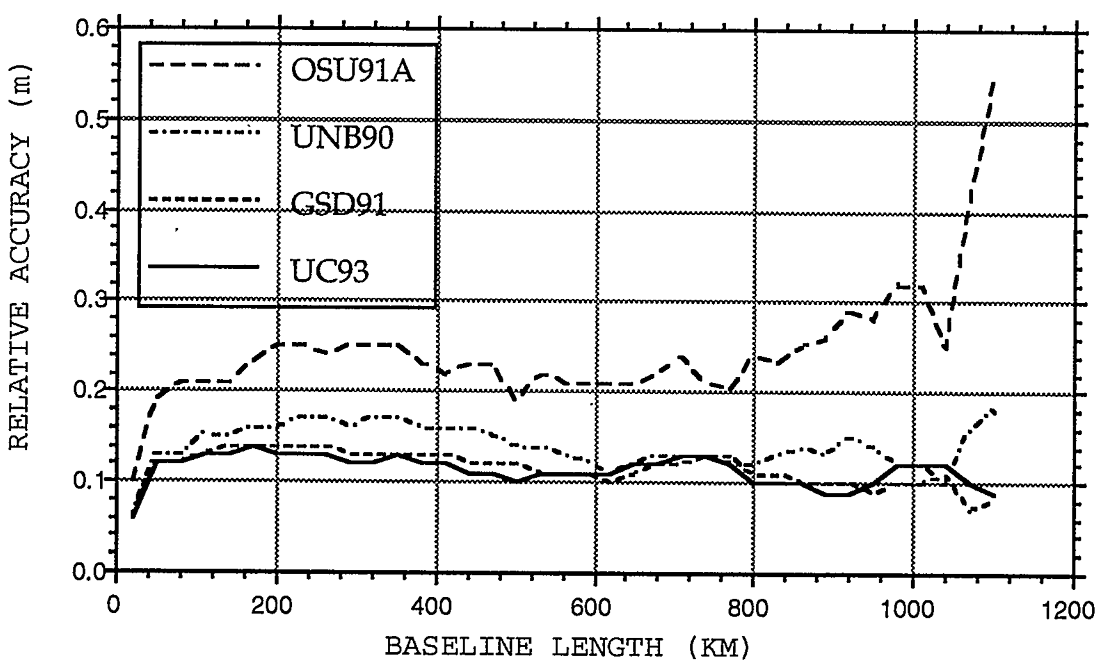

Fiure 6.10b. Relative Undulation Accuracy in Ontario/Quebec (203 Points), in metre

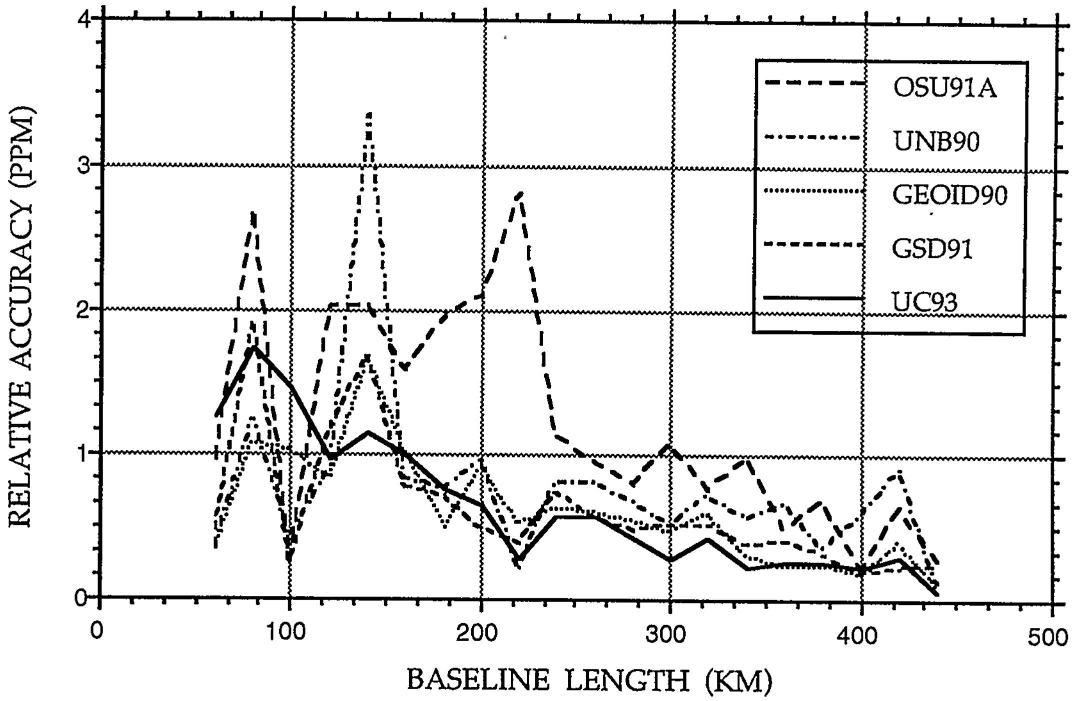

Figure 6.11a. Relative Undulation Accuracy in Oregon State, in ppm

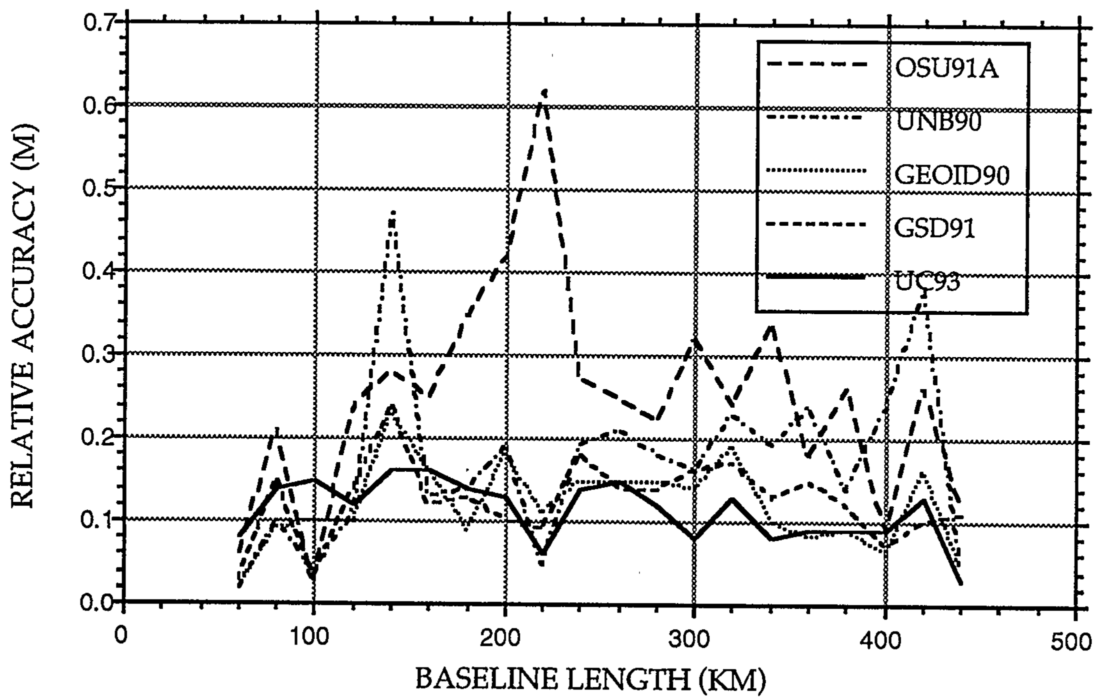

Figure 6.11b. Relative Undulation Accuracy in Oregon State, in metre

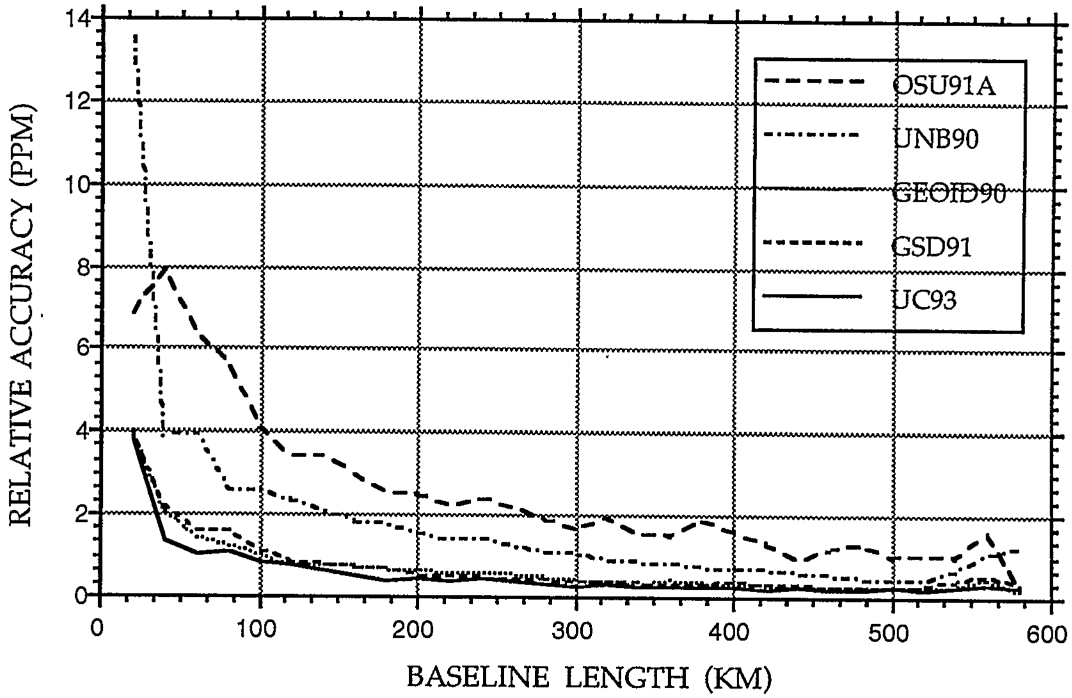

Figure 6.12a. Relative Undulation Accuracy in Washington State, in ppm

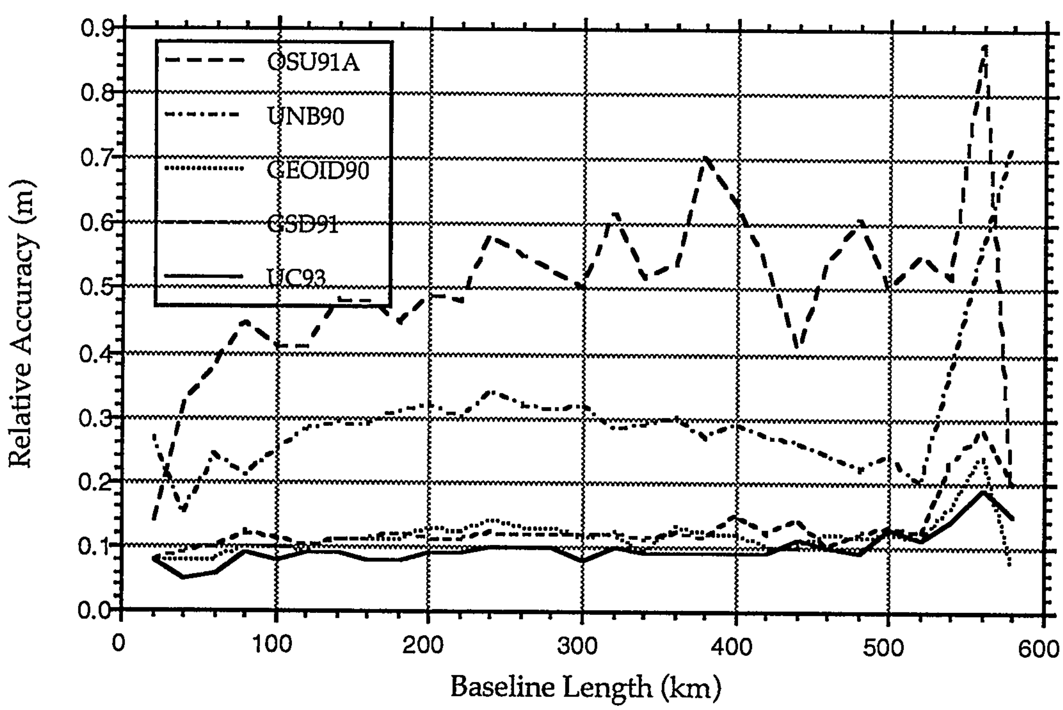

Figure 6.12b. Relative Undulation Accuracy in Washington State, in metre

To compare the above actual relative error estimates with those obtained from error propagation, the relative undulation error contributed by the geopotential model coefficient noise (table 3.2) and the error contributed from gravity measurement noise were combined to generate the internal relative precision of the undulation differences. The contribution of the anomaly noise to the relative undulation is taken approximately as 9 cm, which is obtained by multiplying the mean error of the undulation in the area of BC in table 6.13 by $\sqrt{2}$. Table 6.16 lists the computed relative error estimates for various baseline lengths.

Comparing the results listed in table 16 with those shown in figures 6.3b to 6.12b, one can see that the relative error (1σ) obtained from error propagation increases with the distance. This reflects the overall error behaviour of the GM-implied actual relative geoid error with respect to the GPS/levelling datum, though it exaggerates the magnitude of the error in most cases. However, the internal error estimates can not properly describe the actual relative undulation errors of the regional geoid obtained by combining the geopotential model with local gravity data and height data. The relative error of the regional geoid is quite uniform and basically independent of the distance (see Figures 6.3b to 6.12b).

Table 6.16 The Internal Errors of Relative Undulations Computed by Error Propagation

Linear Distance (km)	Angular Distance (DEG.)	Error Standard Deviation (cm)
10	0.09	12.9
20	0.18	20.2
30	0.27	28.1
40	0.36	35.6
50	0.45	42.3
70	0.63	53.2
90	0.81	60.3
100	0.90	62.6
200	1.80	72.4
400	3.60	77.6
600	5.40	78.2
800	7.19	78.2
1000	8.99	78.3
1600	14.39	77.9
2000	17.99	77.9
10000	89.93	77.9

6.3 Comparison of Different Geoid Models

In terms of comparing different geoid models, the tables and figures listed in the previous two sections indicate that most geoid models show good agreement with the GPS/Levelling data, with UC93 giving the best results.

The addition of local gravity data and height data improves the reference geoid computed from the OSU91 geopotential model significantly, both absolutely and relatively over distances from tens of kilometres to over 1000 km. The improvement is especially large in rough terrain such as the British Columbia area. As shown in tabe 6.2b, the absolute geoidal undulation error drops from 77 cm RMS to 10 cm RMS. The relative undulation errors range from 28 cm to 204 cm over distances of 20 km to about 1500 km for OSU91A geoid model while for the UC93 geoid model the error is only about 12 cm uniformly over all distances (Figure 6.4b). Moreover, the incorporation of local or regional data into the solution removes the possible distance-dependent trend of the undulation error inherent in the geopotential model, as clearly shown in Figure 6.4b.

In relatively flat areas, such as Great Slave Lake and Ontario/Quebec, the geoid file GSD91 which was computed by planar FFT without zero padding is almost as good as the UC93 geoid which is the strict evaluation of the discrete spherical Stokes integral and the UC92 which is the rigorous evaluation of the planar approximation of the Stokes integral. But in mountainous areas, such as the province of British Columbia, the contribution of the errors from planar approximation and edge effects is significant. As shown in table 6.2a, the RMS error of GSD91 is 6 cm higher than that of UC93, and 3cm higher than that of UC92. It is expected that the effect of the FFT edge error will be more severe toward the edges of the grid.

To further study the errors of the various approximate techniques, comparisons were made between the rigorous 1D FFT results and other geoid files computed by approximate methods for the grid points covering all of Canada. Table 6.17 gives the statistics of the comparison results.

Table 6.17. Statistics of the Approximation Errors of Three Geoid Files Computed by 2D FFT With Respect to the Geoid File Computed by the Rigorous 1D Spherical FFT Technique

GEOID FILES	MIN	MAX	MEAN	RMS	σ
	(m)				
NGSD91	-1.928	2.321	0.496	0.718	0.519
UC92_2DP	-0.767	1.508	0.330	0.476	0.343
UC92_2DS	-0.665	1.704	0.248	0.324	0.208

As shown in table 6.17, the combined effects of planar approximation and FFT edge effects is about 72 cm RMS for the GSD91 geoid model . The error caused by planar approximation with the geoid file UC92_2DP, which was computed by planar FFT with proper zero padding, is about 48 cm, indicating that the error caused by edge effects is about 24 cm RMS. As expected, the 2D spherical

FFT approach shows significant improvement over the planar FFT. The RMS error was reduced by about 15 cm as compared to the planar FFT results. But it still has a 32cm RMS error against the true results due to the latitude-dependent error introduced by the modification of the Stokes kernel function in Strang van Hees' approach.

In the two networks in the U.S (Washington and Oregon), the accuracy of GEOID90, which was computed by the 2D spherical FFT technique using a $3' \times 3'$ mean gravity grid, is slightly poorer than that of UC93. As shown in table 6.8 and table 6.9, the RMS error of GEOID90 is 2cm and 1cm higher than that of UC93 (1D FFT). This might be due to the latitude-dependent error caused by the modification of the Stokes kernel in the 2D spherical FFT technique adopted for that computation.

In the Great Slave Lake region and in the Ontario/Quebec area, the UNB90 geoid is at the same level of accuracy as other geoid files. But in all other GPS networks, UNB90 is poorer than other geoid models. In Southern Alberta, the results from UNB90 are even poorer than those of OSU91A (table 6.5a and figure 6.7). One of the possible reasons for the poorer accuracy of UNB90 might be that the geoid was obtained through integration point by point using data in a spherical cap of a certain limited radius (like 6 degrees) around each computation point while the FFT-based technique makes use of all the data on the grid. Another reason might be that a different scheme for terrain reductions (Vanicek and et al., 1990) was adopted for computing the geoid. More research is required to account for the differences.

It should be mentioned that the GPS heights were obtained by fixing the coordinates of one station in each network. Therefore, the GPS heights are referred to the datum defined by this station. To get a better picture of the absolute agreement between the gravimetric geoid and the GPS/levelling implied geoidal undulations, an absolute datum such as that provided by the coordinates of a VLBI or SLR station should be fixed for the network adjustment. It is also worthwhile to make a combined adjustment of all the individual GPS networks in Canada using the above datum for a more comprehensive comparison of the different types of geoidal undulations.

Summarizing the discussions in this chapter, we conclude that the newly computed UC93 geoid model shows the best agreement with the GPS/levelling data available in the region. The absolute agreement is better than 10 cm RMS in most cases and better than 5 cm in areas with mild terrain and good gravity data coverage. The relative agreement is better than 15 cm over distances from tens of kilometres to over 1000 kilometres, showing no significant dependence on the distance as is the case with the geopotential model. Results from regression analyses show that the significant datum difference between the GPS/levelling datum and the gravimetric datum can be reliably removed by just using a few benchmarks (4 stations) occupied by GPS receivers, which is important for GPS-aided levelling projects.

CHAPTER 7

CONCLUSIONS AND RECOMMENDATIONS

The major objectives of this research have been accomplished. A PC based software package, which incorporates the most recent developments in spectral techniques for geoid determination, has been developed. It allows for rigorous evaluation of the discrete Stokes integral, the standard deviations of the computed geoidal undulations contributed from the gravity anomaly data noise, the terrain corrections, and the direct and indirect effects of terrain reductions on the geoid using data on large 2D grids efficiently by the 1D Fast Fourier Transform. The package also includes a program for interpolation and graphical display of the geoid as well as a program for comparing the gravimetric geoid with the GPS/levelling-derived geoidal undulations. The software package can be used for computing large-scale continental geoids efficiently on low cost microcomputers.

With the developed software package, a new high-precision geoid has been computed for all of Canada and part of the U.S. which achieves the best agreement with the GPS/levelling data available in the region as compared to other existing geoids. The comparison of the UC93 geoid with GPS/levelling data shows that the absolute agreement with respect to the GPS/levelling datum (after the systematic datum difference between the gravimetric and the

GPS/levelling-derived undulations is removed) is better than 10 cm RMS, and the relative agreement is better than 15 cm over distances ranging from tens of kilometres to over 1000 kilometres or about 1 to 4 ppm over short baselines of 20 to 100km, 0.5 to 1ppm for distances of 100 to 200km, and 0.1 to 0.5 ppm over distances of 200km to more than 1000 km, in most cases. In some areas with good gravity data coverage and relatively flat terrain, such as Southern Alberta, the absolute agreement is 3 cm and the relative agreement is about 5 cm over distances of 20 km to 500 km.

The UC93 geoid shows significant improvement over other existing geoid models in the test regions. The improvement is especially significant in mountainous areas. In the mountainous Province of British Columbia, the absolute accuracy with respect to GPS/levelling data (203 points) is 10 cm RMS for the UC93 geoid model while it is 15 cm, 71 cm and 77 cm RMS, for the GSD91, the UNB90, and the OSU91A geoid model, respectively. The relative accuracy of the UC93 geoid model is about 12 cm uniformly for distances of 20 km to 1500 km while it is 18 cm for GSD91, 20 cm to 210 cm for UNB90, and 30 cm to 200 cm for OSU91A. The results also indicate that the incorporation of local or regional gravity anomaly data and height data in the geoid determination removes the distance-dependent error inherent in the geopotential model effectively and results in relative geoidal undulations of uniformly high accuracy.

The investigation on the errors of the planar FFT technique and the 2D spherical FFT approach shows that for the determination of large-scale continental geoids the approximation errors of these two methods are quite significant and may lead to severe degradation of the accuracy of the computed geoid. In the area of Canada, the planar FFT technique shows an error as large as 48 cm RMS with respect to the results derived by the rigorous 1D spherical FFT method. The approximation error of the 2D spherical FFT approach also reaches 32 cm RMS. Therefore, the 1D spherical FFT method should be used for computing large-scale continental geoids.

The above agreement of the gravimetric geoid with respect to the GPS/levelling data indicates that the combination of the geoid with GPS heights can generate orthometric heights without levelling with high accuracy for most of the area tested. For areas with moderate terrain and good gravity coverage, such as southern Alberta, better than 5 cm accuracy over distances of 20 km to 500 km can be expected. It must be mentioned that there may exist significant systematic datum difference between the GPS/levelling data and the gravimetric geoid. At least 4 levelling benchmarks should be occupied by GPS receivers to provide datum transformation parameters when the GPS heights are combined with gravimetric geoidal undulations to generate the orthometric heights.

Note that the current accuracy is achieved with a 5' x 5' gravity grid which was compiled using point gravity data with an average separation of about 10 km. However, in areas with relatively good gravity coverage (no data gaps) and moderate terrain, such as Southern Alberta, the accuracy of the UC93 geoid is comparable to the best local geoids available in the world, such as the 1989 geoid model for the Federal Republic of Germany (Denker,1990), which was computed using a 60"x100" gravity grid compiled from point gravity data of an average spacing of 2 km to 5 km, and showed an RMS error of 1 cm to 6 cm with respect to the GPS/levelling data available in that region.

With the improvement of gravity data coverage, density, and quality, which might be realized by modern measurement techniques such as airborne gravimetry in the near future, the realization of cm-accuracy geoids may be achievable. This will, in turn, make it possible to replace costly levelling procedure by GPS and geoid data to generate the orthometric heights (or height differences) with sufficient accuracy for a wide range of applications. More research is required to determine the requirements on the quality and density of gravity measurements as well as other information such as digital terrain model to achieve the goal.

In addition, the combination of different types of data, such as high-degree geopotential models, satellite altimetry data plus sea surface topography model, GPS/leveling data, and surface gravity data, is becoming an important area of research in geoid determination. To combine all data types in an optimal way and to maintain operational efficiency is an intriguing question. Some theoretical and practical problems, such as how to get reliable statistical information on the errors of different data types which are necessary for optimal data combination, how to get rid of gross errors in the data sets, whether to perform the combination in the frequency domain or space domain, etc., are related to this research topic and remain to be investigated. They are recommended for further research.

REFERENCES

Bracewell, R. (1986): The Fourier Transform and Its Applications. 2nd Edition, Revised, McGraw-Hill, New York

Brigham, E.O. (1980): " The Fast Fourier Transform." Prentice-Hall, Inc., Englewood Cliffs, New Jersey, 1988

Christodolidis, Demosthenes C. (1976):" On the Realization of a 10 cm Relative Oceanic Geoid." Report No. 247, Department of Geodetic Science and Surveying, The Ohio State University, Columbus, Ohio 1976

Denker, Heiner (1990):" GPS control of the 1989 Gravimetric Quasigeoid for the Federal Republic of Germany." 106 International Association of Geodesy Symposia, Determination of the Geoid, Present and Future

Forsberg, R. (1990):" A New High-Resolution Geoid of the Nordic Area." 106 International Association of Geodesy Symposia, Determination of the Geoid, Present and Future

Forsberg, R. and M.G. Sideris (1993):" Geoid Computations By the Multi-Band FFT Approach." Accepted to be published in Manuscripta Geodaetica

Haagmans, R.H.N., Erik de Min and M. van Gelderen (1992): " Evaluation of Stokes' and Other Integrals Using 1D_FFT and a Comparison with Existing Methods. " To be published at Manuscripta of Geodetica

Heiskanen, W., and H. Moritz (1967): Physical Geodesy. W. H., Freeman, New York, 1967

Kearsley, A.H.W. (1984): " Precision Limitations and Data Requirements for the Determination of Relative Geoid Heights from Gravimetry." Report No. 26, Department of Geodesy, University of Upsalla, Upsalla, Sweden, 1984

Mainville, A., and Veronneau, M. (1990) " Orthometric Heights Using GPS in Canada." 106 International Association of Geodesy Symposia, Determination of the Geoid, Present and Future

Mainville, A. and M. Veronneau. (1989) " Creating a Gravity Grid Over Canada Using Bouguer Anomalies and a Digital Elevation Model." the Canadian Geophysical Union Annual Meeting, Montreal, Quebec, May, 1989

Milbert, D.G. (1991) " GEOID90: A High-Resolution Geoid for the United States. " EOS, Trans., AGU, vol. 72, no.49,1991

Rapp, R.H., Y.M. Wang and N. Palvis (1991):"Geopotential and Sea Surface topography Harmonic Coefficient Models.". Report No. 410, Department of Geodetic Science and Surveying, The Ohio State University, Columbus, Ohio 1991

Schwarz, K.P. (1984):"Data Types and Their Properties." Proceedings on Local Gravity Approximation, Beijin International Summer School, Beijin, China, 1984

Schwarz, K.P. and M.G. Sideris (1985):" Precise Geoid Heights and Their Use in GPS Interferometry." Geodetic Survey Division Contract Report No. 85-004, E.M.R., Canada

Schwarz, K.P., M.G. Sideris and R. Forsberg (1990) " The Use of FFT Techniques in Physical Geodesy. " Geophs. J. Int., 100, 485-514,1990

Sideris, M.G. (1984): " Computation of Gravimetric Terrain Corrections Using Fast Fourier Transform Techniques." M.Sc. Thesis, Department of Surveying Engineering, University of Calgary

Sideris, M.G. (1987): "Spectral Methods for the Numerical Solution of Molodensky's Problem." PH.D dissertation, Department of Surveying Engineering, University of Calgary

Sideris, M.G., I.N. Tziavos and K.P. Schwarz (1989): Computer Software for Terrain Reductions Using Molodensky's Operator. Geodetic Survey Devision Contract Report No. 89-003, E.M.R., Canada

Sideris, M.G. and K.P. Schwarz (1986): "Improvement of Medium and Short Wavelength Features of Geopotential Solutions by Local Gravity Data." Proceeding of the International Symposium on the Definition of the Geoid, Florence, Italy, May 26-30, 1986

Sideris, M.G. and K.P. Schwarz (1985): Computation of Geoidal Undulations and Deflections of the Vertical for Alberta. Alberta Bureau of Surveying and Mapping Contract Report No. 84004, Edmonton, Alberta, Canada

Sideris, M.G., K.P. Schwarz and A.C. Rauhut (1988a): The Geoid in Northern British Columbia. Geodetic Survey Division Contract Report No. 88-004, E.M.R., Canada

Sideris, M.G., K.P. Schwarz and A.C. Rauhut (1988b): The Geoid in Northern British Columbia. Geodetic Survey Division Contract Report No. 88-004, E.M.R., Canada

Sideris, M.G. and Y. Li (1992): " Improved Geoid Determination for Levelling by GPS" , the sixth Int. Geodetic Symposium on Satellite Positioning", Columbus, OH, March 17- 20, 1992

Sjoberg, L.E.(1984):" Least Squares Modification of Stokes' and Vening-Meinesz Formulas by Accounting for Truncation and Potential Coefficient Errors." Manuscripta Geodaetica, Vol.9, 1984

Sjoberg, L.E.(1986):" Comparison of Some Methods of Modifying Stokes' Formula." Bull. Geod. Sci. Aff., 45, 3, 1986

Sjoberg, L.E.(1991):"Refined Least Squares Modification of Stokes' Formula." Manuscripta Geodaetica, 15, 4, 1990

Strang van Hees, G., (1986):"Precision of the geoid, computed from terrestrial gravity measurements." Manuscripta Geodaetica, vol. 11, No. 1, 1986

Strang van Hees, G., (1990):"Stokes formula using Fast Fourier Techniques." Manuscripta Geodaetica, Vol. 11, 1990

Vanicek, P., A. Kleusberg, R-G. Chang, H. Fashir, N. Christo, N. Hofman, T. Kling, and T. Arsenault, (1986):" The Canadian Geoid." Geodetic Survey Division Contract Report No. 86-001, E.M.R., Canada, 1986

Vanicek, P., Peng Ong and Zhang Changyou (1990): " New Gravimetric Geoid for Canada: The " UNB 90" Solution." 106 International Association of Geodesy Symposia, Determination of the Geoid, Present and Future

Veronneau, M. and A. Mainville (1992): " Computation of a Canadian Geoid Model Using the FFT Technique to Evaluate Stokes' and Vening-

Meineza' Formulas in a Planar Approximation." Paper presented in the AGU spring Meeting, Montreal, 1992

Wichiencharoen, C. (1982):" The Indirect Effect on the Computation of Geoid Undulations." Report No. 336, Department of Geodetic Science and Surveying, The Ohio State University, Columbus, Ohio 1982

Yan Min Wang (1993):" On the Optimal Combination of the Potential Coefficient Model with the Terrestrial Gravity Data for the Geoid Computations." To be published in Manuscripta Geodaetica